Chemical Science

ROYAL SOCIETY OF CHEMISTRY

REVIEW

View Article Online
View Journal | View Issue

Cite this: *Chem. Sci.*, 2026, **17**, 772

Cross-scale understanding of cascade electrocatalysis for carbon and nitrogen utilization

Shiping Li,[a] Youyu Pang,[ab] Hongmei Li,[a] Rui Yang,[c] Zhaoyu Jin,[c] Guihua Yu *[d] and Panpan Li *[a]

Cascade electrocatalysis is increasingly being recognized as a promising approach for achieving efficient and selective conversion of carbon and nitrogen resources, in response to critical challenges in energy sustainability and environmental management. Compared to conventional single-site systems, cascade pathways are designed to enable spatial and temporal coordination of multiple reaction steps, through which the generation, migration, and transformation of key intermediates can be precisely controlled. In this review, a multiscale perspective is provided, spanning atomic, sub-nanoscale, nanoscale, and macroscopic dimensions. Recent progress is summarized in several representative strategies, including the use of multiple active sites for relay catalysis, the engineering of crystal facets and heterointerfaces, the application of nanoconfinement, and the implementation of tandem reactor systems. Particular emphasis is placed on their applications in CO_2 reduction, nitrate reduction, and urea electrosynthesis. Moreover, state-of-the-art *in situ* characterization techniques are highlighted, through which dynamic insights into catalyst evolution and intermediate behaviour have been obtained. Finally, opportunities are outlined for future development, where rational catalyst design, integrated system construction, and data-driven optimization are expected to further advance cascade electrocatalysis for sustainable chemical transformations.

Received 19th November 2025
Accepted 8th December 2025

DOI: 10.1039/d5sc09063f

rsc.li/chemical-science

[a]*College of Materials Science and Engineering, Sichuan University, Chengdu, 610065, China. E-mail: panpanli@scu.edu.cn*

[b]*College of Materials Science and Engineering, Chongqing Jiaotong University, Chongqing, 400074, China*

[c]*Institute of Fundamental and Frontier Sciences, University of Electronic Science and Technology of China, Chengdu 611731, China*

[d]*Materials Science and Engineering Program, Walker Department of Mechanical Engineering, The University of Texas at Austin, Austin, Texas, 78712, USA. E-mail: ghyu@austin.utexas.edu*

Guihua Yu

Dr Guihua Yu is John J. McKetta Centennial Energy Chair in Engineering, Temple Foundation Endowed Professor of Materials Science and Engineering and Mechanical Engineering at The University of Texas at Austin, affiliated with Texas Materials Institute, UT Energy Institute and UT Chemistry. He received his BS degree in chemistry with the highest honor from USTC, PhD in chemistry from Harvard University, followed by postdoc research at Stanford. He has been focusing on the rational design of polymeric materials and hybrid organic–inorganic nanomaterials, fundamental understanding of their chemical and physical properties, and exploration of their applications in environment, energy, and sustainability technologies.

Panpan Li

Dr Panpan Li is a Professor at Sichuan University. She received her BS in Chemistry, MEng. in Environmental Engineering, and PhD in Environmental Science from Sichuan University. She was a postdoctoral scholar at the University of Texas at Austin starting from 2019. She joined Sichuan University as a faculty member and established her independent research group in late 2021. Her research focuses on innovative materials and electrochemical technologies for environmental and energy sustainability.

Introduction

Carbon and nitrogen cycles are fundamental processes that govern Earth's climate regulation and resource metabolism.[1–3] However, intensified human activities have profoundly disturbed the equilibrium of these two cycles. In the case of the nitrogen cycle, although the traditional Haber–Bosch process can effectively reduce nitrogen to synthesize ammonia, its high temperature and pressure requirements not only result in enormous energy consumption but also cause severe environmental impacts.[4,5] In contrast, electrochemical approaches, which can achieve the reaction under mild conditions and directly utilize renewable electricity, are considered as more sustainable alternatives. Nevertheless, electrochemical nitrogen reduction suffers from low efficiency due to the strong N≡≡≡N bond strength (945 kJ mol^{-1}) and resultant high reaction overpotentials.[6–8] Nitrate, with its lower N–O bond dissociation energy, is more readily reduced electrochemically and is viewed as a promising alternative nitrogen source for ammonia synthesis.[9,10] Similarly, the carbon cycle plays a crucial role in addressing climate change and global warming, but excessive CO_2 emissions have intensified the greenhouse effect, creating an urgent demand for carbon capture and conversion technologies. CO_2 electroreduction, as a potential carbon resource utilization method, has emerged as a research focus.[11,12] However, both CO_2 and NO_3^- electroreduction reactions involve complex multistep reaction pathways and face challenges such as slow reaction kinetics, poor selectivity, and high energy barriers.[13] Due to thermodynamic and kinetic limitations, traditional single-step electrochemical reduction processes lack sufficient control over key intermediates, thereby leading to low utilization rates and poor product selectivity, which severely hampers the efficient and directional conversion of carbon and nitrogen resources.

Cascade electrocatalysis, a strategy that converts reactants through multiple reaction steps, provides a new approach to address carbon and nitrogen resource utilization challenges. Cascade electrocatalysis refers to the integration of multiple electrocatalytic reaction steps in space and time, where different active sites sequentially transform intermediates, thus overcoming the thermodynamic and kinetic constraints of a single reaction step.[14,15] In microbes, the conversion of NO_3^- to NH_3 is a cascade reaction: nitrate reductase reduces NO_3^- to NO_2^-, which is then further reduced to NH_3 by nitrite reductase or nitrogenase.[16–18] Inspired by this, researchers have started applying cascade electrocatalysis to carbon and nitrogen resource utilization. Cascade electrocatalysis allows multiple electrocatalytic reactions to occur in series on a single catalyst surface or within a reaction system, not only overcoming the thermodynamic and selectivity limitations in nitrogen and carbon conversion but also significantly improving reaction efficiency and product selectivity.[19,20] Current research on cascade electrocatalysis primarily focuses on studies at a single scale, such as investigating single-atom catalysis mechanisms at the atomic scale. While such studies help to elucidate the reaction mechanisms of individual active sites, they face numerous limitations, such as limited compatibility of single active sites and hindered interfacial mass transfer. To address these limitations, cross-scale cooperative effects have drawn increasing attention. In cascade catalytic systems, structural features and reaction behaviors at different scales are closely coupled. At the atomic scale, active sites govern the adsorption and transformation pathways of key intermediates. At the nanoscale, interfacial and confinement structures regulate intermediate migration, short-range spillover, and the local reaction microenvironment. At the reactor scale, mass-transfer rates, electrolyte distribution, and pH collectively dictate overall reaction kinetics and efficiency[21,22] Integrating these multiscale strategies enables precise control over the spatiotemporal distribution of reaction intermediates, thereby establishing an efficient and selective cascade pathway for complex multistep reactions. However, this cross-scale research also faces challenges, including the limitations of multiscale modeling and characterization techniques, the complexity of reaction mechanisms, and the challenges of material design. Through a deeper understanding and optimization of cascade electrocatalysis mechanisms at multiple scales, future advancements could offer viable solutions to the global energy crisis and environmental pollution issues.

This review provides a comprehensive assessment of the mechanisms and applications of cascade electrocatalysis from a multiscale perspective (Fig. 1). It begins by elucidating the reaction mechanisms underlying cascade electrocatalysis, encompassing atomic, sub-nanoscale, nanometer, and macroscopic scales. The review then highlights *in situ* characterization techniques employed to study cascade electrocatalysis. Subsequently, it summarizes key advancements in cascade electrocatalytic strategies, including multiple active sites, crystal facets and heterointerfaces, nanoconfinement and tandem reactors with a particular focus on their application in the utilization of carbon and nitrogen resources, such as nitrate reduction reaction (NO_3RR), carbon dioxide reduction reaction (CO_2RR), and urea synthesis. Finally, the challenges facing the field of cascade

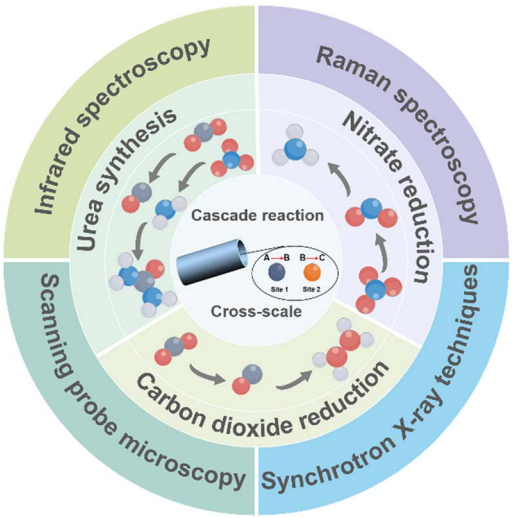

Fig. 1 Cascade electrocatalysis for carbon and nitrogen utilization.

electrocatalysis are discussed, along with a forward-looking perspective on its future prospects, aiming to promote the development of cascade electrocatalysis in the field of electrochemical technologies.

Cross-scale strategies for cascade electrocatalysis

Cascade electrocatalytic reactions, involving sequential transformations, hold immense potential for efficient resource conversion. However, their mechanistic complexity remains a formidable challenge. At the atomic scale, catalytic behaviour is dictated by single-atom effects and synergistic interactions between multi-atom sites. At the nanoscale, catalytic performance relies on the interplay between surface structure and reactant dynamics. Given the diversity of intermediates and their varied migration pathways, single-scale analyses are insufficient to capture the full mechanistic landscape. Therefore, a comprehensive multiscale approach is indispensable for elucidating the formation, transformation, and coupling of intermediates, thereby laying a robust theoretical foundation for cascade electrocatalysis. This section systematically explores the mechanisms at the atomic, sub-nanoscale, nanoscale, and macroscopic levels (Fig. 2), highlighting the distinct contributions of each to cascade processes.

Atomic scale: single-atom and dual/multi-atom site interactions

Cascade electrocatalysis achieves high efficiency through consecutive reactions, with atomic-scale insights proving pivotal for optimizing both selectivity and conversion. At this scale, single-atom and dual- and multi-atom site effects govern catalytic performance. Single-atom catalysts (SACs) utilize isolated metal atoms as active centers, exploiting their distinct electronic structures and maximizing atomic utilization to enhance reaction kinetics and selectivity.[23] In the NO_3RR, SACs provide well-defined active sites and efficient electron transfer pathways, thereby lowering energy barriers and accelerating reaction rates.[24–27] Li *et al.*[28] developed a copper-based single-atom gel (Cu SAGs) catalyst that selectively adsorbs and activates nitrite intermediates at single-atom sites during the cascade NO_3RR. This configuration effectively suppresses the competing hydrogen evolution reaction (HER), enabling highly selective NO_3^- to NH_3 conversion under neutral conditions. This work demonstrates the synergistic integration of pulse electrolysis and three-dimensional (3D) structured SAGs, facilitating highly efficient NO_3^- to NH_3 conversion *via* tandem catalysis of otherwise unfavorable intermediates.

Beyond single-atom effects, dual- and multi-atom catalysts leverage cooperative interactions between adjacent metal centers to modulate intermediate adsorption and migration, thereby enhancing both activity and selectivity.[29–31] In the CO_2RR and NO_3RR, such bimetallic sites can establish energetically favorable tandem pathways.[32] For instance, Xie *et al.*[33] reported a MOF-supported Pd–Cu bimetallic catalyst that promotes CO_2 to C_{2+} conversion through a tandem mechanism: Cu facilitates *CO adsorption and C–C coupling, while Pd stabilizes $*CH_2CHO$ intermediates, achieving a C_{2+} faradaic efficiency (FE) of 81.9%. Similarly, Yan *et al.*[34] designed a Cu–Ni bimetallic MOF catalyst where Cu reduces NO_3^- to NO_2^-, and Ni subsequently converts NO_2^- to NH_3. Although SACs exhibit high atom utilization and selectivity, their isolated nature limits the cooperative interactions crucial for multistep transformations.[35] In contrast, dual- and multi-atom configurations enable spatially adjacent, functionally complementary active centers that facilitate sequential intermediate conversion and minimize diffusion losses.[36,37]

Sub-nanoscale: interfacial effects

At the sub-nanoscale, interfacial effects arising from charge redistribution and atomic coordination at boundaries between distinct catalytic phases play a pivotal role in intermediate stability, charge transfer kinetics, and reaction selectivity.[38] These interfacial regions can significantly influence reaction pathways by modulating local electronic structures and adsorption energetics.[39] Metal–metal interfaces often exhibit catalytic behavior that differs markedly from that of their individual components. As demonstrated by Zhang *et al.*,[40] a well-designed Cu/Ag interface promotes asymmetric CO–CHO coupling: Ag domains generate *CO intermediates, while the

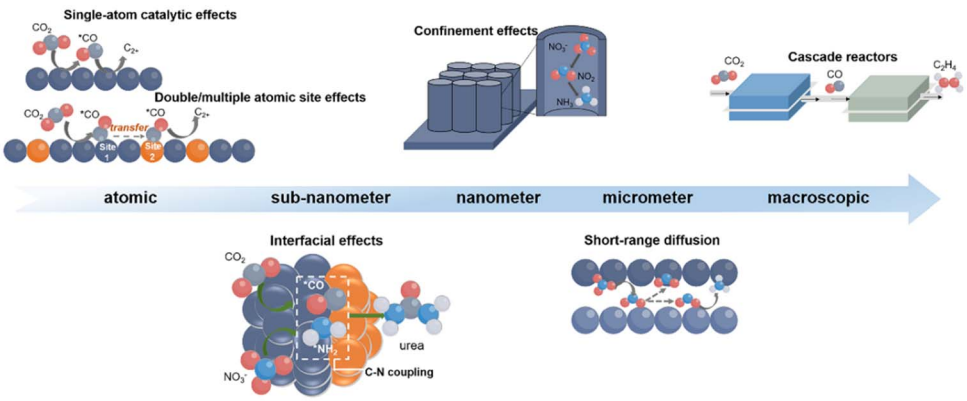

Fig. 2 Mechanistic study of cascade electrocatalytic reactions.

Cu/Ag interface concurrently suppresses the HER, favors *CO hydrogenation to *CHO, and enhances C_2H_4 formation. Similarly, metal–support interactions can substantially tune electronic states and surface reactivity. Xu *et al.*[41] developed a MOF-derived CuPd/N-doped carbon nanoarrays catalyst, wherein interfacial charge polarization between the metal sites and carbon support facilitates an efficient cascade pathway for the NO_3RR to NH_3.

Nanoscale: confinement effects

Confinement effects in nanostructured catalysts create spatially restricted environments that enhance reactant-site interaction frequency and minimize diffusion distances.[42,43] This spatial confinement accelerates reaction kinetics while suppressing side reactions, thereby improving selectivity.[44] For instance, Qiu *et al.*[45] validated this concept in a nanoconfinement-based cascade denitrification system, utilizing pulsed photocatalysis to mediate chlorine spillover within TiO_2 nanotubes integrated with CuO_x. In this confined environment, cathodically generated NH_4^+ and photogenerated chlorine radicals ($^{\bullet}Cl$) are localized in close proximity. The spillover of $^{\bullet}Cl$ facilitates the selective oxidation of NH_4^+ to N_2. This approach demonstrates highly efficient treatment of nitrate-contaminated wastewater and holds great promise for the removal of complex nitrate pollutants from water bodies in future applications.

Macroscopic scale: reactor cascading

At the macroscopic scale, cascade electrocatalysis can be engineered through reactor-level integration, where sequential reactions are spatially separated into interconnected electrolyzers. In these systems, the first cell produces intermediates that are subsequently converted in downstream reactors under optimized conditions of potential, pH, and electrolyte composition.[46] This modular approach enables precise reaction control and enhanced product selectivity. Ozden *et al.*[47] developed a two-step CO_2 to C_2H_4 system that integrates a solid oxide electrolyzer cell (for CO_2 to CO conversion) with a membrane electrode assembly (for CO to C_2H_4 reduction). This configuration minimizes CO_2 loss to carbonate formation and reduces total energy consumption by nearly 48%, achieving efficient ethylene synthesis. Moreover, hybrid cascade systems can further integrate electrochemical, thermocatalytic, or biocatalytic processes. For example, Xia *et al.*[48] presented a tandem electrothermal-catalytic system that efficiently utilizes cathodic CO and anodic O_2 products in the CO_2RR, converting arylboronic acids and amines into valuable organic amides within a tandem thermocatalytic reactor. This study demonstrates the feasibility of a tandem electrothermal-catalytic strategy for achieving CO_2 conversion and amide synthesis. It offers a novel pathway for comprehensively exploiting CO_2 electrolysis. In addition, Han *et al.*[49] presented a spatially decoupled electrobiological system that first utilizes tannic acid-Cu^{2+} metal-phenolic networks to electrocatalytically convert CO_2 into ethanol. Subsequently, engineered *Escherichia coli* ferment the ethanol into itaconic acid, isopropanol, and polyhydroxybutyrate, achieving efficient conversion of CO_2 into high-value chemicals.

Advanced *in situ* techniques for probing cascade reactions

In cascade electrocatalytic reactions, the intricate and interdependent nature of successive reaction steps demands precise coordination among active sites. Achieving a comprehensive understanding of both the underlying reaction mechanisms and the catalyst's performance under working conditions is therefore essential. *In situ* characterization techniques serve as powerful, real-time analytical tools, enabling the direct observation of reaction dynamics. These techniques provide direct insights into the evolution of catalyst surface microstructures and reaction processes, thereby furnishing critical experimental evidence that can inform the optimization of catalytic performance and the design of advanced catalysts. This section highlights several widely utilized *in situ* techniques and underscores their pivotal contributions to advancing cascade electrocatalysis research.

Synchrotron X-ray techniques

Synchrotron X-ray techniques, particularly X-ray absorption spectroscopy (XAS), have found extensive application in elucidating the electronic structure, oxidation states, and local coordination environments of catalysts (Fig. 3a). Specifically, *in situ* extended X-ray absorption fine structure (EXAFS) analysis enables the tracking of variations in the coordination environments of absorbing atoms under reaction conditions, thus facilitating the determination of atomic coordination states. Concurrently, *in situ* X-ray absorption near-edge structure (XANES) offers insights into potential-dependent chemical state changes.[50–52] In cascade electrocatalysis, XAS is instrumental in monitoring valence state evolution within tandem catalysts across multiple reaction stages, thereby providing mechanistic insights for each step.[53] For instance, Lou *et al.*[54] employed XAS to quantitatively analyze the atomic structure of a Janus Cu@Ni catalyst (Fig. 3b and c). EXAFS confirmed the distinct Cu- and Ni-enriched domains, while XANES, in conjunction with XPS, revealed electron transfer from Ni to Cu. These findings corroborated a tandem mechanism, wherein NO_3^- adsorption and activation occur on Cu sites, while H species generated on Ni sites migrate to the interface, facilitating N–O bond cleavage. Such studies elucidate the intrinsic nature of multi-site synergy and cascade reaction mechanisms at the electronic level, advancing our understanding of the coupling between charge transfer and reaction pathways in catalytic processes.

Infrared spectroscopy

Fourier-transform infrared spectroscopy (FTIR) detects molecular vibrations *via* infrared absorption at characteristic frequencies, offering real-time, molecular-level insights into the chemical species involved in electrocatalytic processes.[57,58] Fig. 3d illustrates a schematic of the FTIR setup. Within cascade electrocatalytic systems, this technique allows for the direct

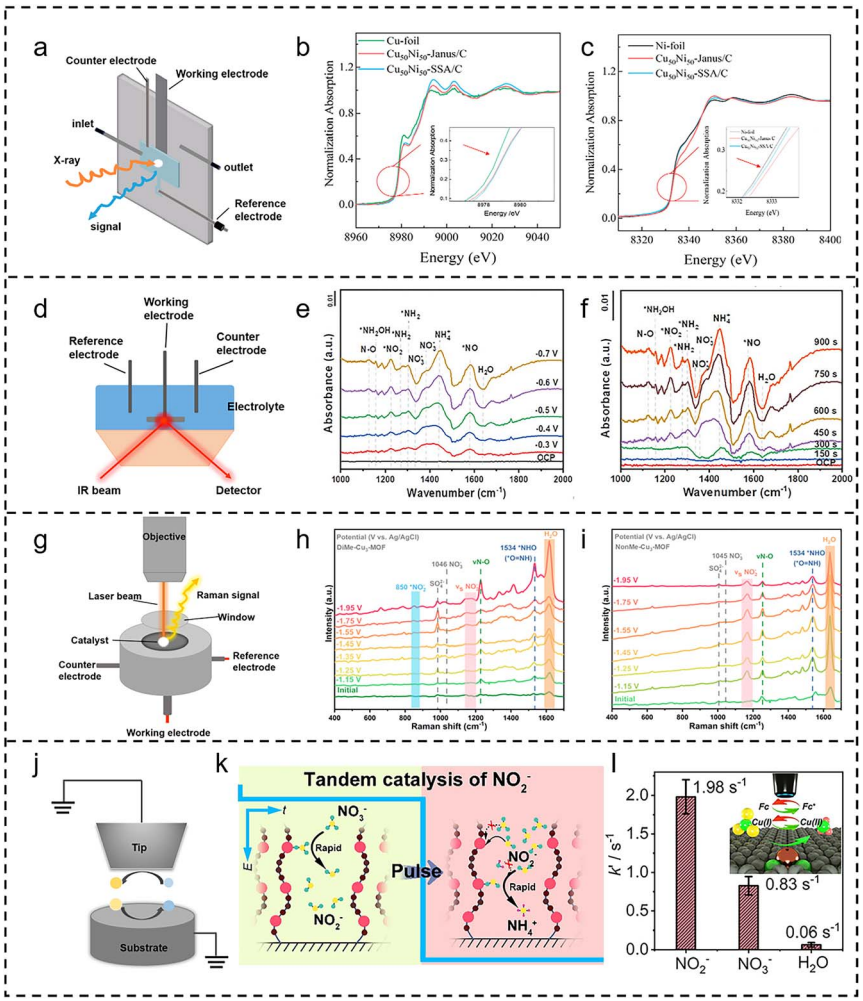

Fig. 3 *In situ* characterization techniques. (a) Schematic diagram of *in situ* XAS. (b) Cu K-edge and (c) Ni K-edge XANES spectra of $Cu_{50}Ni_{50}$-Janus/C, $Cu_{50}Ni_{50}$-SSA/C, and reference samples. Reproduced with permission.[54] Copyright 2024, American Chemical Society. (d) Schematic diagram of *in situ* FTIR spectroscopy. *In situ* FTIR spectra of $Cu_5/Mo_{0.6}WO_3$ (e) from OCP to −0.7 V *vs.* RHE, and (f) from OCP (0 s) to 900 s at −0.7 V *vs.* RHE. Reproduced with permission.[55] Copyright 2025, Wiley-VCH. (g) Schematic diagram of *in situ* Raman spectroscopy. *In situ* Raman spectra of (h) DiMe-Cu_3-MOF and (i) NonMe-Cu_3-MOF at various applied potentials in 50 mM KNO_3 and 0.5 M K_2SO_4 electrolytes. Reproduced with permission.[56] Copyright 2025, Royal Society of Chemistry. (j) Schematic diagram of *in situ* SECM. (k) Schematic diagram of the NO_3RR *via* pulse electrolysis cascade catalysis. (l) Kinetic rate constants of NO_2^-, NO_3^-, and H_2O adsorption on Cu SAGs determined with SI-SECM. Reproduced with permission.[28] Copyright 2023, American Chemical Society.

monitoring of adsorbed reactants, intermediates, and products on electrode surfaces, facilitating the identification of intermediate species within the cascade pathway and their transformation processes. When integrated with complementary techniques, FTIR can effectively track the formation, conversion, and consumption of key intermediates, offering crucial evidence for understanding reaction kinetics, electron transfer, and molecular interactions.[59] Dai *et al.*[55] utilized FTIR to confirm the cascade mechanism of a Cu/Mo-WO_3 catalyst, dynamically capturing the spectral evolution of key intermediates. The depletion of certain peaks and the emergence of new ones provided real-time evidence of NO_3^- reduction to NO_2^- and subsequent conversion to NH_3, validating the proposed stepwise mechanism (Fig. 3e and f). Such real-time spectral tracking under *operando* conditions underscores the power of FTIR in unraveling complex cascade reaction pathways.

Raman spectroscopy

Raman spectroscopy, which integrates laser excitation with electrochemical measurements, provides valuable information on chemical composition and molecular structure by detecting characteristic shifts in scattered light (Fig. 3g).[60,61] This technique offers real-time tracking of intermediates, enabling the precise tracking of pathway changes in complex cascade reactions.[62] Such molecular-level insight is essential for correlating structural dynamics with the optimization of catalytic performance. For instance, Fu *et al.*[56] utilized Raman spectroscopy to monitor the characteristic peaks of the NHO intermediate and dynamic Cu–N bond variations on DiMe-Cu_3-MOF and NonMe-Cu_3-MOF surfaces (Fig. 3h and i). Based on the Raman results, the *NHO intermediate was detected on both DiMe-Cu_3-MOF and NonMe-Cu_3-MOF, whereas the *NOH intermediate was not

detected, indicating that NO_3^- is reduced to NH_3 *via* the NHO pathway. Combined with DFT calculations, the results revealed a 0.32 eV reduction in the energy barrier for $*NO_2$ to $*NO_2H$ conversion through hydrogen bonding, thus optimizing the cascade pathway toward highly selective and industrially relevant NO_3RR to NH_3 conversion.

Scanning probe microscopy

Scanning electrochemical microscopy (SECM) is a high-resolution *in situ* electrochemical imaging technique that enables the study of local surface reactivity with micrometer spatial and millisecond-scale temporal resolution (Fig. 3j).[63,64] Using micro- or nanoelectrode probes, SECM quantifies current responses between the probe and the substrate, allowing real-time mapping of localized reaction activity, kinetics, and intermediate distribution.[65] In cascade electrocatalysis, SECM is particularly useful for visualizing how intermediates form and dissipate at different active sites. For example, in NO_3RR and CO_2RR, SECM has been employed to track key intermediates such as NO_2^- and CO, elucidating reaction coupling between spatially separated active centers.[66–68] He *et al.*[69] utilized the surface generation-tip collection (SG-TC) mode to detect NO_2^- and NH_3 formed on a Cu/$Co(OH)_2$ model catalyst during NO_3^- electroreduction. NH_3 generation significantly increased at the Cu-$Co(OH)_2$ interface, accompanied by a marked decrease in NO_2^- production. These results confirmed that NO_2^- preferentially forms on Cu sites and subsequently diffuses to adjacent $Co(OH)_2$ sites, where it undergoes further reduction to NH_3 *via* a tandem process. In another study, Li *et al.*[28] employed surface interrogation scanning electrochemical microscopy (SI-SECM) to demonstrate that a Cu SAG catalyst exhibited a substantially higher adsorption affinity for NO_2^- than for NO_3^- or H_2O (Fig. 3k and l). This finding established a potential-dependent cascade mechanism, where intermediate accumulation was observed at low potentials followed by efficient conversion to NH_3 at high potentials, enabling highly efficient NO_3RR.

In addition to these techniques, *in situ* electron microscopy, such as liquid-cell transmission electron microscopy (TEM), is emerging as a powerful approach for visualizing catalyst structural evolution during electrochemical reactions.[70–72] While its application to cascade electrocatalysis remains limited, it holds significant promise. However, current *in situ* characterization methods still face notable limitations. Their temporal and spatial resolutions are often insufficient to fully capture the short-lived intermediates and transient changes at nanoscale active sites during cascade reactions, and it remains challenging to simultaneously resolve the dynamic evolution of catalyst structures and reaction intermediates. Given the strong

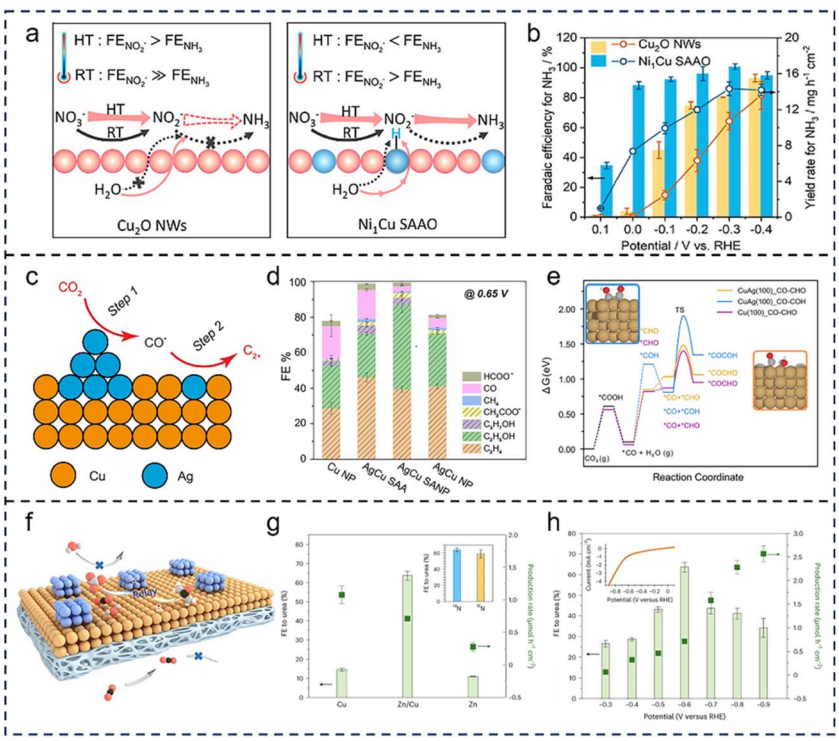

Fig. 4 Relay catalysis with multiple active sites. (a) Schematic diagram of the electrothermal synergistic effect of Cu_2O NWs and Ni_1Cu SAAO in the NO_3RR process. (b) FE and yield of NH_3 for Cu_2O NWs and Ni_1Cu SAAO at different applied potentials. Reproduced with permission.[94] Copyright 2024, American Chemical Society. (c) Scheme of the cascade catalysis mechanism over AgCu SANP. (d) FE results of Cu NP, AgCu SAA, AgCu SANP, and Ag NP catalysts toward the CO_2RR at −0.65 V. (e) Comparison of the C–C coupling activation barrier for the *CHO (on CuAg and pure Cu) and *COH intermediates (CuAg). Reproduced with permission.[96] Copyright 2023, Springer Nature. (f) Mixed catalyst design where one component (blue) lowers the activation energy for C–N bond formation, and the second component (orange) reduces the activation energy for protonation steps required for urea formation. (g) Zn/Cu hybrid catalyst and its single-component counterparts for urea FE. (h) FE and yield of urea on the Zn-0.5/Cu hybrid catalyst at different applied potentials. Reproduced with permission.[1] Copyright 2023, Springer Nature.

complementarity among different *in situ* techniques, a comprehensive understanding of cascade electrocatalytic mechanisms requires the combined use of multiple *in situ* methods to compensate for individual weaknesses and to investigate the reaction from distinct temporal and spatial perspectives. For example, coupling synchrotron-based X-ray methods with *in situ* vibrational spectroscopy enables the concurrent tracking of catalyst structural evolution and the formation and consumption of intermediates. Moreover, advancing *in situ* techniques with higher temporal and spatial resolution, such as ultra-high-resolution SECM, will provide powerful tools for probing mechanistic pathways in greater detail.

Recent progress on cascade electrocatalysis

Carbon and nitrogen resource utilization is a pivotal link in advancing sustainable energy and green chemistry.[73–75] However, typical CO_2RR, NO_3RR, and their coupled reactions often involve multi-electron/proton transfers and the dynamic migration of various reaction intermediates. This presents a series of challenges, including sluggish reaction kinetics, complex competitive pathways, and low product selectivity.[22,76–84] Traditional single-step electrocatalysis often suffers from intermediate accumulation, low energy efficiency, and limited product selectivity in these reactions. In contrast, cascade electrocatalysis, where multiple reaction steps are spatially and temporally integrated, offers a new avenue for efficient carbon–nitrogen resource utilization by enabling effective intermediate generation, transport, and transformation. This section discusses recent advancements in cascade electrocatalytic systems targeting carbon and nitrogen resource conversion.

Relay catalysis with multiple active sites

The strategy of relay catalysis with multiple active sites leverages the different selectivities of various sites for specific reaction steps, decoupling elementary steps within complex reaction

Table 1 Summary of multiple active site catalysts

Catalyst	Mechanism	Electrolyte	Potential	FE
Cu_2O–CoPO-2 (ref. 88)	Cu_2O: $NO_3^- \rightarrow NO_2^-$ CoPO: $H_2O \rightarrow$ *H	0.1 M NO_3^- + 1.0 M KOH	−0.37 V *vs.* RHE	95%
Ru–Ni nanosheets (ref. 89)	Ru: $NO_3^- \rightarrow$ *HONO Ni: *HONO + *H $\rightarrow NH_3$	0.1 M K_2SO_4 + 0.002 M KNO_3	−0.8 V *vs.* RHE	96%
TTA–TPH–CuCo (ref. 98)	Cu: $NO_3^- \rightarrow NO_2^-$ Co: $NO_2^- \rightarrow NH_3$	0.5 M K_2SO_4 + 0.3 M KNO_3	−0.75 V *vs.* RHE	92%
$Ag_{30}Pd_4$ nanocluster (ref. 93)	Ag: $NO_3^- \rightarrow NO_2^-$ Pd: $NO_2^- \rightarrow NH_3$	1.0 M NaOH + 1500 ppm NO_3^-–N	−0.6 V *vs.* RHE	90%
Ni1Cu single-atom alloy oxide nanowires (ref. 94)	Ni: $H_2O \rightarrow$ *H Cu: *NO_x + *H $\rightarrow NH_3$	1.0 M KOH + 0.1 M KNO_3	+ 0.1 V *vs.* RHE	80%
Mo_1Fe_1Pd dual single-atom alloy (ref. 99)	Mo: $NO_3^- \rightarrow NO_2^-$ Fe: $NO_2^- \rightarrow NH_3$	1.0 M KNO_3 + 1.0 M KOH	−0.7 V *vs.* RHE	94%
AgCu single-atom and nanoparticle (ref. 96)	Ag NP: $CO_2 \rightarrow$ CO AgCu SAA: C–C coupling	1.0 M KOH	−0.65 V *vs.* RHE	94%
0.2% CoCu single-atom alloy (ref. 100)	Co: $CO_2 \rightarrow$ CO Cu: C–C coupling	1.0 M $KHCO_3$	−1.01 V *vs.* RHE	51%
Cu_3N–Ag nanocubes (ref. 97)	Ag: $CO_2 \rightarrow$ CO Cu: CO $\rightarrow$ *CHO $\rightarrow C_2H_4$	1.0 M KOH	−0.7 V *vs.* RHE	50%
CuO/Ni single atoms (ref. 101)	Ni: $CO_2 \rightarrow$ CO Cu: CO $\rightarrow C_{2+}$	1.0 M KOH	−0.892 V *vs.* RHE	81%
CoCu composite (ref. 102)	Co: $CO_2 \rightarrow$ CO Cu: CO $\rightarrow C_2H_5OH$	0.1 M $KHCO_3$	−0.8 V *vs.* RHE	71%
Mo_1Cu single-atom alloy (ref. 103)	Mo: $H_2O \rightarrow$ *H Cu^0: $CO_2 \rightarrow$ CO $Cu^{\delta+}$: C–C coupling	1.0 M KOH	−1.7 V *vs.* RHE	86%
Zn/Cu hybrid catalyst (ref. 1)	Zn: stabilize CO_2NO_3 Cu: lower the protonation barrier of $COOHNH_2$	0.1 M $KHCO_3$ + 500 ppm NO_3^-–N	−0.6 V *vs.* RHE	75%
Zn_1/In_2O_{3-x} (ref. 83)	In-OV: $CO_2 \rightarrow$ *CO Zn_1-OV: $NO_3^- \rightarrow NH_2$	0.1 M $KHCO_3$ + 0.1 M KNO_3	−0.7 V *vs.* RHE	56%
Fe_1/MoS_2 (ref. 104)	Fe_1–S_3: *CO_2NO_2 $\rightarrow$ * CO_2NH_2 MoS_2: *CO_2NH_2 $\rightarrow$ *$COOHNH_2$	0.1 M $KHCO_3$ + 0.1 M KNO_3	−0.5 V *vs.* RHE	55%
Mo–PCN-222(Co) (ref. 105)	Co: $CO_2 \rightarrow$ *CO Mo: $NO_3^- \rightarrow NH_2$	0.1 M $KHCO_3$ + 50 mM KNO_3	−0.4 V *vs.* RHE	34%
$CuPd_1Rh_1$ diatomic alloy (ref. 106)	Pd_1–Cu: *CO_2NO_2 $\rightarrow$ * CO_2NH Rh_1–Cu: *CO_2NH_2 $\rightarrow$ *$COOHNH_2$	0.1 M $KHCO_3$ + 0.1 M KNO_3	−0.5 V *vs.* RHE	72%
CuSn composite (ref. 107)	Cu: $CO_2 \rightarrow$ *CO Sn: $NO_3^- \rightarrow NH_2$	0.1 M KNO_3	−0.7 V *vs.* RHE	79%

networks in space. This approach utilizes the cooperative effect between sites to integrate each reaction step in a relay fashion, optimizing the functional complementarity and energy matching between active sites, thereby significantly enhancing overall reaction efficiency and product selectivity.[85,86] In the typical multi-electron and multi-proton transfer process of the NO_3RR, researchers have successfully achieved precise regulation of reaction pathways and directional transformation of intermediates by rationally designing multiple active site catalysts, significantly improving catalytic performance and opening new avenues for the development of efficient NO_3RR processes.[87–92] For instance, Qin *et al.*[93] designed an atomically precise $Ag_{30}Pd_4$ bimetallic nanocluster, where Ag sites preferentially adsorb NO_3^- and efficiently convert it into NO_2^- intermediates. Subsequently, the NO_2^- intermediate migrates directionally to the adjacent Pd sites for deep reduction to the final product NH_3. This study decoupled the NO_3RR steps and allocated them to Ag and Pd sites, achieving high FE for NH_3 production (>90%). Furthermore, external field control can effectively enhance the relay catalysis of the NO_3RR *via* multiple active sites. For instance, Liu *et al.*[94] designed a Ni-modified copper oxide single-atom alloy (Ni_1Cu SAAO) catalyst, which achieved efficient NO_3RR to NH_3 *via* a thermally-coupled electrocatalytic strategy. The cascade reaction mechanism, shown in Fig. 4a, involved heating (60–80 °C), which significantly promoted the hydrolysis of Ni single-atom sites to generate active hydrogen. These active hydrogens were relayed to neighboring Cu sites, accelerating the hydrogenation of NO_x intermediates (*e.g.*, NO_2) adsorbed on the Cu surface, thereby overcoming the kinetic barriers of NO_x hydrogenation and the competition with the HER. This catalyst exhibited optimized NH_3 production performance at elevated temperatures, with a FE of approximately 80% and a rate of 9.70 mg h^{-1} cm^{-2} (Fig. 4b).

In addition, relay catalysis with multiple active sites can significantly promote key processes such as C–C coupling and C–N coupling, enabling the efficient synthesis of high-value multi-carbon or nitrogen-containing compounds.[95] Du *et al.*[96] reported an Ag–Cu bimetallic catalytic system that demonstrated exceptional performance in the CO_2RR. In this system, Ag nanoparticles efficiently reduced CO_2 to CO, while the Ag sites induced compression strain in the Cu lattice, enhancing the adsorption energy of the *CO intermediate on the Cu sites and significantly promoting C–C coupling kinetics, thereby achieving a high FE for multi-carbon products (94%) (Fig. 4c–e). Similarly, Luo *et al.*[1] designed a Zn/Cu bimetallic catalyst that further extended the application of tandem catalysis in C–N coupling reactions. As shown in Fig. 4f, the Zn sites preferentially stabilized the key C–N coupling intermediate CO_2NO_3, while the Cu sites relayed the reduction of the $COOHNH_2$ protonation energy barrier. This strategy successfully optimized the reaction pathway and suppressed side reactions, achieving 75% selectivity in simulated wastewater containing 1000 ppm

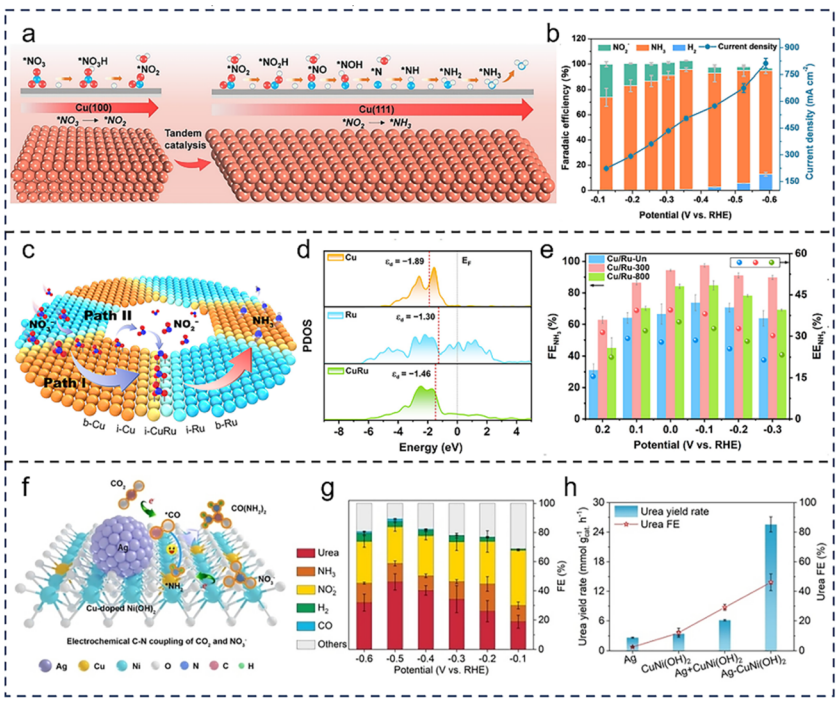

Fig. 5 Crystal facet and heterointerface coupling in cascade catalysis. (a) Synergistic effects between Cu(100) and Cu(111) crystal facets. (b) Total current density and FE of different products on Cu nanosheets. Reproduced with permission.[111] Copyright 2023, Wiley-VCH. (c) Schematic illustration of the proposed mechanism for NO_3^- to NH_3 conversion on the Cu/Ru HHNS. (d) Projected density of states (PDOS) for b-Cu, b-Ru, and i-CuRu. (e) FE_{NH_3} and EE_{NH_3} of Cu/Ru-Un, Cu/Ru-300, and Cu/Ru-800 across a potential range of 0.2 to −0.3 V_{RHE}. Reproduced with permission.[112] Copyright 2025, American Chemical Society. (f) Schematic diagram of CO_2 and NO_3^- co-reduction to urea on the Ag-$CuNi(OH)_2$ electrocatalyst. (g) FE of possible products from the Ag-$CuNi(OH)_2$ composite material. (h) Comparison of urea yield and FE between Ag NPs, $CuNi(OH)_2$ NSs, their physical mixture, and Ag-$CuNi(OH)_2$. Reproduced with permission.[113] Copyright 2024, Wiley-VCH.

NO_3^- (Fig. 4g and h). In summary, multi-active-site catalysts can sequentially activate different reactants and intermediates based on the selective specificity of different sites toward reaction steps. This enables them to regulate the energy barriers and pathways of key steps, thereby achieving tandem catalysis for complex reactions. However, cascade strategies based on multiple active sites still face limitations. These include insufficient microenvironmental compatibility between sites, restricted migration of reaction intermediates, and the structural complexity of catalysts, which complicates mechanistic analysis and undermines stability.[97] Integrating multiscale approaches can help align individual steps more effectively and thereby improve the overall efficiency and stability of cascade reactions. Table 1 summarizes the catalytic processes of various multiple active site catalysts. This strategy provides important theoretical and experimental paradigms for the design of high-performance cascade catalytic systems and the high-value conversion of carbon and nitrogen cycles.

Crystal facet and heterointerface coupling

The crystal facet and heterointerface cascade catalysis enhances the overall catalytic efficiency by constructing functionally complementary active regions, which collaboratively guide the orientation and coupling of reaction pathways. This synergy optimizes the multiple step reaction energy barriers and the

Table 2 Summary of crystal facet and heterointerface-based cascade catalysts

Catalyst	Mechanism	Electrolyte	Potential	FE
Cu nanosheets (ref. 111)	Cu(100): $NO_3^- \rightarrow NO_2^-$ Cu(111): $NO_2^- \rightarrow NH_3$	1.0 M KOH + 0.2 M KNO_3	−0.59 V *vs.* RHE	88%
Cu/Ru hollow heteronanostructure (ref. 112)	Cu: $NO_3^- \rightarrow NO_2^-$ Cu/Ru: $NO_2^- \rightarrow NH_3$	0.1 M KNO_3 + 0.1 M KOH	−0.1 V *vs.* RHE	97%
4H/fcc Au–Cu heterostructures (ref. 117)	4H/fcc Au: $NO_3^- \rightarrow NO_2^-$ 4H/fcc Cu: $NO_2^- \rightarrow NH_3$	1.0 M KOH + 1.0 M KNO_3	−0.6 V *vs.* RHE	98%
CuO@CeO_{2-x} heterostructured nanotubes (ref. 118)	Amorphous CuO: $NO_3^- \rightarrow NO_2^-$ Cu–Ce: $NO_2^- \rightarrow NH_3$	0.1 M KOH + 0.01 M KNO_3	−0.4 V *vs.* RHE	96%
c-Co_3O_4/a-CuO heterostructure (ref. 119)	a-CuO: $NO_3^- \rightarrow$ *NO_2 c-Co_3O_4: *$NO_2 \rightarrow NH_3$	0.2 M K_2SO_4 + 0.1 M NO_3^-	−0.8 V *vs.* RHE	90%
Ni@Cu_{2-x}Se nanoarrays (ref. 120)	$Cu_{2-x}Se$: $NO_3^- \rightarrow NO_2^-$ Interface: modulating *H Ni: $H_2O \rightarrow$ *H	1.0 M KOH + 0.1 M KNO_3	−0.4 V *vs.* RHE	91%
CoO–CuO_x heterostructure (ref. 121)	CuO_x: $NO_3^- \rightarrow$ *NO_2 Interface: promoting the transfer of electrons CoO: *$NO_2 \rightarrow NH_3$	0.5 M Na_2SO_4 + 200 ppm $NaNO_3$–N	−0.5 V *vs.* RHE	92%
Ag–Cu heterostructure (ref. 116)	Ag: $NO_3^- \rightarrow NO_2^-$ Interface: facilitating the spillover of intermediates Cu: $NO_2^- \rightarrow NH_3$	0.1 M KOH + 0.1 M KNO_3	−0.5 V *vs.* RHE	>80%
SnO_2/Cu_6Sn_5/CuO nanocatalysts (ref. 122)	Cu_6Sn_5/SnO_2: $CO_2 \rightarrow$ *CO_2^- Cu_6Sn_5/CuO: $H_2O \rightarrow$ *H	0.5 M $NaHCO_3$	−0.95 V *vs.* RHE	90%
Ag/Cu self-evolution tandem catalysts (ref. 123)	Ag: $CO_2 \rightarrow CO$ Interface: enhancing the adsorption of intermediates Cu: $CO \rightarrow C_{2+}$	1.0 M KOH	−1.8 V *vs.* RHE	89%
Au–Cu heterostructure (ref. 124)	AuCu: $CO_2 \rightarrow CO$ Cu: $CO \rightarrow C_{2+}$	0.1 M $KHCO_3$	−0.75 V *vs.* RHE	—
Au/Cu heterostructure (ref. 125)	Au (110): $CO_2 \rightarrow$ *CO Cu(110): $CO \rightarrow C_{2+}$	0.1 M $KHCO_3$	−0.75 V *vs.* RHE	—
Cu_2O nanoparticle (ref. 126)	(100): $CO_2 \rightarrow$ *CO; C–C coupling (111): C_2H_4 overflow	0.2 M KI	−1.3 V *vs.* RHE	57%
Ag–Cu Janus nanostructures (ref. 127)	Ag domains: $CO_2 \rightarrow CO$ Cu domains: $CO \rightarrow C_{2+}$	0.1 M $KHCO_3$	−1.2 V *vs.* RHE	72%
Ag–Cu biphasic heterostructure (ref. 128)	Ag: $CO_2 \rightarrow CO$ Interface: promoting the transport of intermediates Cu: $CO \rightarrow C_{2+}$	0.1 M $KHCO_3$	−1.05 V *vs.* RHE	44%
Cu/Cu_2O heterostructures (ref. 129)	Cu^0: $NO_3^- \rightarrow$ *NH_2; C–N coupling Interface: promoting the transport of intermediates Cu^+: *$CH_3CNHCOO^- \rightarrow$ *$CH_3CHNH_2COO^-$	0.5 M KNO_3; 0.2 M PA	−0.6 V *vs.* RHE	75%
Ag–Cu composite (ref. 130)	Ag: $CO_2 \rightarrow CO$ Interface: promoting the transport of intermediates Cu: $CO \rightarrow C_{2+}$	3.0 M KOH	−1.0 V *vs.* RHE	80%

mass transfer of intermediates, ultimately improving catalytic performance. The facet-based cascade strategy involves tuning the exposed crystal facets of the catalyst, leveraging the distinct catalytic properties arising from variations in atomic arrangement, coordination, and electronic structure across different facets. These properties enable the selective catalysis of specific reaction steps.[108–110] Fu *et al.*[111] proposed a crystal facet cascade catalysis strategy, where the Cu(100) and Cu(111) facets cooperatively perform tandem catalysis (Fig. 5a). The Cu(100) facet preferentially adsorbs NO_3^- and efficiently reduces them to NO_2^-, while the NO_2^- intermediate migrates to the adjacent Cu(111) facet for the hydrogenation step. This catalyst achieves a current density of 665 mA cm^{-2} for NH_3 production and a rate of 1.41 mmol h^{-1} cm^{-2} in a flow cell under −0.59 V *vs.* RHE (Fig. 5b), significantly enhancing the NO_3RR to NH_3 performance.

In contrast, the heterointerface cascade strategy capitalizes on the unique local atomic and electronic environments created at the interfaces of different materials due to lattice mismatch, electronic interactions, and other factors. These environments facilitate the effective adsorption and activation of reactants and intermediates.[114,115] For example, Chen *et al.*[112] demonstrated a Cu/Ru heterointerface shell–core nanocavity catalyst that enabled efficient cascade electroreduction of NO_3^- to NH_3, significantly enhancing the reaction rate and selectivity (Fig. 5c–e). NO_3^- is first adsorbed and reduced to NO_2^- at the Cu site, after which NO_2^- desorbs and accumulates in the nanocavity. The accumulated NO_2^- is rapidly transferred to the Cu/Ru

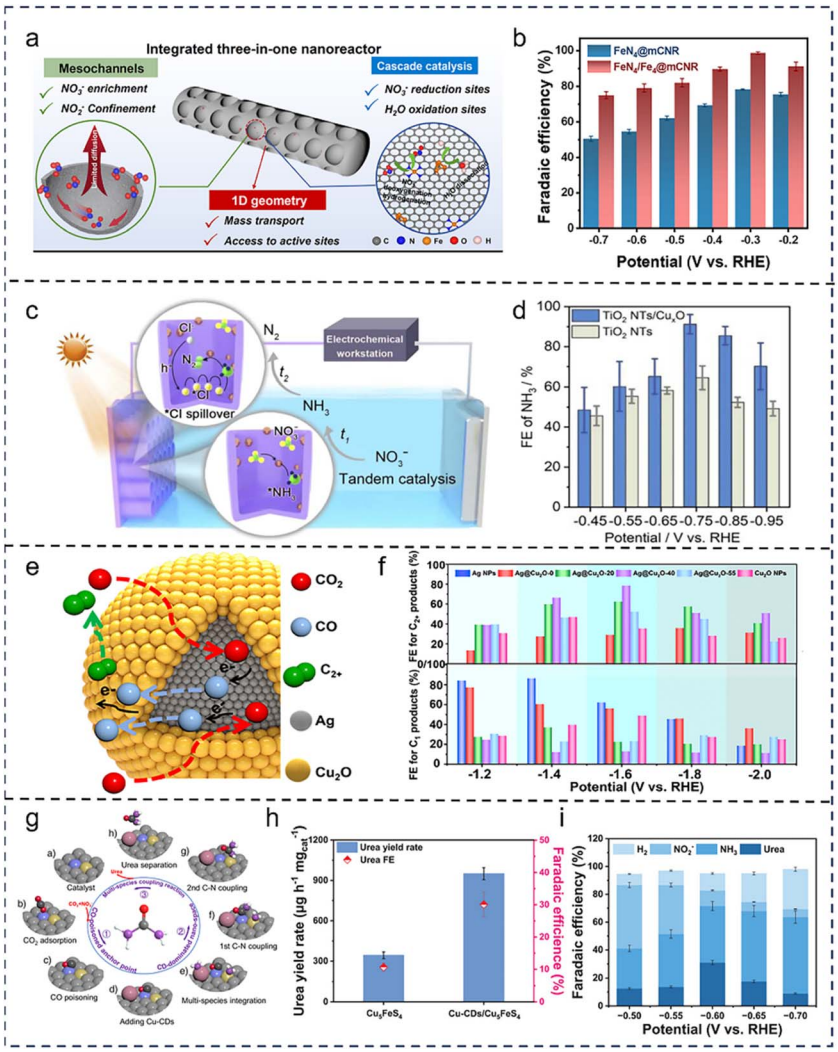

Fig. 6 Nanoconfinement in cascade catalysis. (a) Schematic illustration of the three-in-one nanoreactor design to accelerate NO_3RR to NH_3 synthesis. (b) FE_{NH_3} of FeN_4@mCNR and FeN_4/Fe_4@mCNR at varied potentials. Reproduced with permission.[135] Copyright 2025, American Chemical Society. (c) Schematic illustration of NO_3^--to-N_2 process *via* the pulsed photoelectrolysis-mediated reactive chlorine spillover process. (d) FE of NH_3 for TiO_2 NTs and TiO_2 NTs/CuO_x. Reproduced with permission.[45] Copyright 2025, Elsevier B.V. (e) Schematic illustration of the confinement catalysis mechanism in Ag@Cu_2O cascade nanoreactors. (f) FE for C_{2+} and C_1 products at various applied potentials. Reproduced with permission.[136] Copyright 2024, American Chemical Society. (g) The Cu-CDs/Cu_5FeS_4 multisite nanoreactor for stepwise multiple species coupling to synthesize urea within the CDs-dominated nano-space *via* utilizing the CO poisoning effect. (h) Urea yield rate and FE of Cu_5FeS_4 and Cu-CDs/Cu_5FeS_4. (i) FE of urea, NH_3, NO_2^-, and H_2 of Cu-CDs/Cu_5FeS_4 in the H-cell. Reproduced with permission.[137] Copyright 2025, Wiley-VCH.

heterointerface, where it undergoes further reduction to NH_3. The Cu/Ru heterointerface facilitates electron transfer from Cu to Ru, improving the adsorption and activation of reaction intermediates at the interface, thus enhancing the utilization of NO_2^- intermediates. Moreover, the heterointerface cascade strategy can also be employed to regulate the generation and conversion of active hydrogen intermediates, facilitating C–N coupling reactions for the synthesis of complex carbon–nitrogen compounds. For instance, Ye *et al.*[113] designed an Ag-$CuNi(OH)_2$ heterostructure that efficiently catalyzed urea electrosynthesis. As shown in Fig. 5f, at the Ag site of the Ag-$CuNi(OH)_2$ catalyst, CO_2 is reduced to the critical *CO intermediate, while at the $CuNi(OH)_2$ site, NO_3^- is reduced to the $*NH_2$ intermediate. These intermediates spontaneously couple at the adjacent heterointerface to form urea, while the interface also optimizes the H_2O splitting process to provide active hydrogen atoms. The Ag-$CuNi(OH)_2$ composite material achieved an impressive urea production rate of 25.6 mmol g^{-1} h^{-1} and a FE of 46% (Fig. 5g and h). The cascade catalysis *via* crystal facets and heterointerfaces allows precise control over reaction pathways and intermediate transformations, substantially enhancing the overall efficiency and selectivity of cascade reactions. This approach offers valuable insights into the efficient use of carbon- and nitrogen-based resources and the sustainable synthesis of green chemicals. Although this strategy holds potential for enhancing cascade reaction efficiency, its practical implementation remains constrained. Differences in adsorption selectivity between crystal facets and interfacial charge redistribution can impede the transfer of intermediates across interfaces. In addition, interfacial reconstruction or fluctuations in the local environment during operation may disrupt the stability of the cascade process.[116] Employing multiscale strategies can reinforce interfacial stability, strengthen the coupling between reaction steps, and improve system scalability, offering new pathways for practical deployment. Table 2 summarizes the catalytic processes of crystal facet and heterointerface-based cascade catalysts.

Nanoconfinement

Nanoconfinement involves constructing nanoreactors or confined spaces that impose spatial constraints on reactants and intermediates, effectively orchestrating multistep reactions within a limited volume. Confined cascade catalysis capitalizes on these spatial constraints to enhance intermediate retention and proximity, leading to higher reaction rates and selectivity.[131–134] For example, Li *et al.*[135] designed a trifunctional nanoreactor system with a 1D geometry, open mesoporous channels, and synergistic active sites for the highly efficient electrocatalytic NO_3RR to NH_3 (Fig. 6a and b). The system uses one-dimensional mesoporous carbon as a support, creating a unique microenvironment that favors NO_3^- transport and adsorption while restricting the diffusion of NO_x intermediates.

Table 3 Summary of the confined cascade catalytic systems

Catalyst	Mechanism	Electrolyte	Potential	FE
FeN_4/Fe_4 mesoporous carbon nanorod (ref. 135)	Fe–N_4: $NO_3^- \rightarrow NO_2^-$ NO_2^- confinement Fe_4: $H_2O \rightarrow *H$	0.1 M NO_3^- + 1.0 M KOH	−0.3 V *vs.* RHE	92%
CuFe@CuNi composite (ref. 140)	CuFe LDH: $NO_3^- \rightarrow NO_2^-$ NO_2^- confinement CuNi LDH: $NO_2^- \rightarrow NH_3$	0.1 M Na_2SO_4 + 50 ppm NO_3^-–N	−1.4 V *vs.* Ag/AgCl	100%
($CoPc-NH_2$ + $NiPc-OCH_3$)/ carbon nanotubes (ref. 141)	$NiPc-OCH_3$: $CO_2 \rightarrow CO$ CO confinement $NiPc-OCH_3$: $CO \rightarrow CH_3OH$	0.1 M $KHCO_3$	−0.98 V *vs.* RHE	50%
Ni sodalite topology/NC (ref. 142)	NiN_3: $CO_2 \rightarrow CO$ CO confinement Cu NPs: $CO \rightarrow C_2H_4$	0.5 M $KHCO_3$	−0.72 V *vs.* RHE	62%
Ag@Cu_2O cascade nanoreactor (ref. 136)	Ag core: $CO_2 \rightarrow CO$ CO confinement Cu_2O shell: $CO \rightarrow C_{2+}$	0.1 M $KHCO_3$	−1.6 V *vs.* RHE	78%
CoPc/carbon nanotubes (ref. 44)	CoPc-out: $CO_2 \rightarrow CO$ CO confinement CoPc-in: $CO \rightarrow CH_3OH$	0.1 M $KHCO_3$	−0.96 V *vs.* RHE	41%
Ag@Cu_2O-*x* nanoreactors (ref. 143)	Ag core: $CO_2 \rightarrow CO$ CO confinement Cu_2O shell: $CO \rightarrow C_{2+}$	1.0 M KOH	−1.2 V *vs.* RHE	74%
Ag–Cu nanoporous bimetallic catalyst (ref. 144)	Ag: $CO_2 \rightarrow CO$ CO confinement Cu: $CO \rightarrow C_{2+}$	0.2 M $KHCO_3$	−1.2 V *vs.* RHE	73%
Cu-CDs/Cu_5FeS_4 nanoreactor (ref. 137)	Fe: $CO_2 \rightarrow CO$ C and N intermediate confinement Cu: $NO_3^- \rightarrow *NH_2$	0.1 M KNO_3	−0.35 V *vs.* RHE	42%
CuCo@N-doped microporous hollow carbon spheres (ref. 145)	Co: $CO_2 \rightarrow CO$ C and N intermediate confinement Cu: $NO_3^- \rightarrow *NH_2$	0.05 M KNO_3 + 0.1 M $KHCO_3$	−0.55 V *vs.* RHE	32%

Simultaneously, the iron single-atom sites (Fe–N_4) and iron nanoclusters (Fe_4) embedded within the support synergistically control the electronic structure to dominate the reduction of NO_3^- and the oxidation of H_2O, respectively. This system demonstrates excellent NO_3RR performance under both alkaline and neutral conditions. Qiu *et al.*[45] confined the intermediate product (NH_4^+) and the active chlorine species (•Cl) within localized regions using TiO_2 nanotubes (Fig. 6c and d). Leveraging the spillover effect of •Cl, they achieved the highly efficient and directed conversion of NH_4^+ to N_2. Furthermore, by precisely controlling the structure of the nanoreactor, the confinement effect can be enhanced, promoting the formation, diffusion, and subsequent utilization of reaction intermediates. For instance, Lu *et al.*[136] synthesized a series of Ag@Cu_2O cascade nanoreactors with tunable shell thicknesses, where the Cu_2O shell thickness was precisely controlled to achieve spatial confinement of the CO intermediate (Fig. 6e and f). In this system, the Ag core efficiently generates the CO intermediate, which, upon escaping, is confined within the porous Cu_2O shell, significantly increasing the local CO concentration and thus promoting C–C coupling to form C_{2+} products. This study not only proposes an effective strategy for fine-tuning the local CO concentration through precise control of the Cu_2O shell thickness but also provides important theoretical insights into the confinement catalysis mechanisms within cascade nanoreactors.

Moreover, confined cascade catalysis can effectively control the accumulation behavior of toxic intermediates, converting them into beneficial factors and enabling complex reactions involving multiple species.[138] For example, Zhang *et al.*[137] designed a nanoreactor composed of copper-carbon dots (Cu-CDs) and chalcopyrite (Cu_5FeS_4) for the efficient synthesis of urea (Fig. 6g–i). In this system, Cu-CDs provide confined nanospaces that stabilize *CO intermediates, preventing CO poisoning of the Fe sites. Meanwhile, two structurally distinct Cu sites facilitate the activation and transformation of nitrogen-containing species, driving the continuous C–N coupling steps and ultimately enabling efficient urea synthesis. This system achieved a urea yield of 1131.84 μg h^{-1} mg_{cat}^{-1} with a selectivity of 42%, significantly enhancing the thermodynamic and kinetic advantages of multiple site synergy and multiple species integration in urea synthesis. These examples demonstrate that nanoscale confinement can markedly influence cascade catalysis by spatially constraining and locally enriching reactive

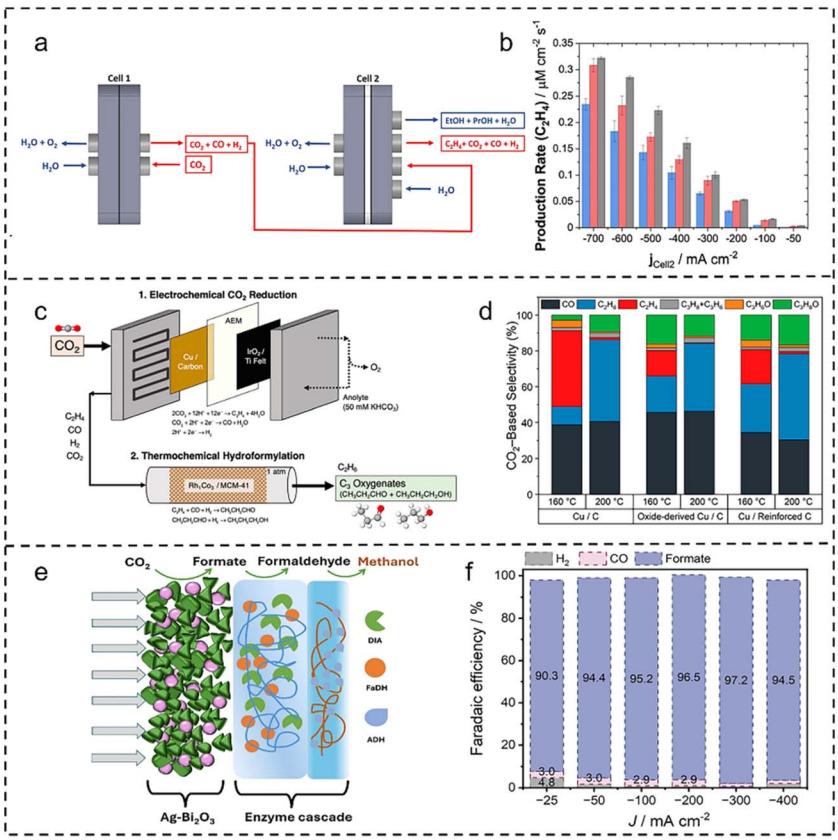

Fig. 7 Tandem reactors. (a) Schematic diagram of the tandem CO_2 electrolyzer. (b) Comparison of C_2H_4 yield between the tandem electrolyzer cascade structure and a single electrolyzer. Reproduced with permission.[147] Copyright 2023, Springer Nature. (c) Tandem electrochemical-thermochemical reactors for CO_2 conversion to C_3 oxygenate products. (d) CO_2-based selectivity of products for 5 cm^2 Cu/C, oxide-derived Cu/C, and Cu/reinforced C cathodes at −220 mA cm^{-2} in combination with 160 and 200 °C hydroformylation temperatures. Reproduced with permission.[149] Copyright 2022, American Chemical Society. (e) Hybrid electrocatalytic-bioelectrocatalytic cascade integrated on a gas diffusion electrode for the CO_2RR under selective formation of methanol. (f) FE for the CO_2RR performed with a GDE constituted of Ag-Bi_2O_3 nanofibers on a hydrophobic carbon paper. Reproduced with permission.[150] Copyright 2025, Wiley-VCH.

intermediates, thereby promoting desired cascade pathways while suppressing side reactions. Designing catalysts with intrinsic nanoscale confinement or incorporating external confined architectures, such as porous frameworks or core–shell structures, has thus become a key strategy for enhancing the performance of cascade electrocatalytic systems.

Table 4 Summary of tandem reactors

Cascade system	Catalyst	Mechanism	Electrolyte	Reaction conditions
Electrochemical–electrochemical	Ni–N–C; Cu (ref. 147)	Cell-1: $CO_2 \rightarrow CO$	Cell-1: 0.1 M $KHCO_3$	Cell-1: 200 mA cm^{-2}
		Cell-2: $CO \rightarrow C_{2+}$	Cell-2: 1.0 M $KHCO_3$	Cell-2: 700 mA cm^{-2}
	Graphite flakes (ref. 148)	Cell-1: $CO_2 \rightarrow$ ethanol	Cell-1: 1.0 M KOH	Cell-1: −1.8 V *vs.* SCE
		Cell-2: ethanol → DEE	Cell-2: 0.5 M H_2SO_4 ethanol solution	Cell-2: 20 mA cm^{-2}
	3D single-atom Ni; Cu_2O (ref. 152)	Cell-1: $CO_2 \rightarrow CO$	Cell-1: 0.5 M $KHCO_3$	Cell-1: 140 mA cm^{-2}
		Cell-2: CO → *n*-propanol	Cell-2: 1.0 M KOH	Cell-2: 42.5 mA cm^{-2}
	Solid-oxide electrolysis cell; m embrane electrode assembly (ref. 47)	Cell-1: $CO_2 \rightarrow CO$	Cell-1: 30 wt% aqueous ethanolamine	Cell-1: 815 mA cm^{-2}
		Cell-2: $CO \rightarrow C_2H_4$	Cell-2: 3.0 M KOH	Cell-2: 150 mA cm^{-2}
	Ni–N–C; Cu nanoparticle (ref. 153)	Cell-1: $CO_2 \rightarrow CO$	Cell-1: 0.5 M K_2SO_4 + H_2SO_4	Cell-1: 5 A
		Cell-2: $CO \rightarrow C_{2+}$	Cell-2: 0.5 M KOH	Cell-2: 4 A
	Ni–Cu; Cu–Al (ref. 154)	Cell-1: $CO_2 \rightarrow CO$	Cell-1: 1.0 M KOH	Cell-1: 400 mA cm^{-2}
		Cell-2: $CO \rightarrow C_{2+}$	Cell-2: 1.0 M KOH	Cell-2: 300 mA cm^{-2}
Electrochemical–thermochemical	Cu; Rh_1Co_3/MCM-41 (ref. 149)	Cell-1: $CO_2 \rightarrow C_2H_4$	Cell-1: 50 mM $KHCO_3$	Cell-1: 220 mA cm^{-2}
		Cell-2: $C_2H_4 \rightarrow C_3$	Cell-2: —	Cell-2: 160, 200 °C
	Pd/C; FeCo (ref. 155)	Cell-1: $CO_2 \rightarrow CO$	Cell-1: 50 mM $KHCO_3$	Cell-1: 150 mA cm^{-2}
		$H_2O \rightarrow H_2$ Cell-2: CO_2, $H_2 \rightarrow$ CNF	Cell-2: —	Cell-2: 450 °C
	Ag-hexamethylenetetramine/Ni-hydroxide carbonate; Pd(II) (ref. 48)	Cell-1: $CO_2 \rightarrow CO$	Cell-1: 0.5 M $KHCO_3$	Cell-1: −0.8 V *vs.* RHE
		$H_2O \rightarrow H_2$ Cell-2: CO_2, $O_2 \rightarrow$ organic amides	Cell-2: —	Cell-2: 120 °C
	$Rh/Sm_xCe_{1-x}O_{2-\delta}$ (ref. 156)	Cell-1: $H_2O \rightarrow H_2$	Cell-1: acceptor-doped $LaGaO_3$	Cell-1: 300–500 mA cm^{-2}
		Cell-2: $CO_2 + CH_4 \rightarrow CO + H_2$	Cell-2: —	Cell-2: 800 °C
	Membrane electrode assembly; Ga/ZSM-5/P (ref. 157)	Cell-1: $CO_2 \rightarrow C_2H_4$	Cell-1: 0.5 M $KHCO_3$	Cell-1: 200 mA cm^{-2}
		Cell-2: $C_2H_4 \rightarrow$ BTEX	Cell-2: —	Cell-2: 600 °C
Electrochemical-biocatalytic	Ag-Bi_2O_3; dehydrogenase (ref. 150)	Cell-1: $CO_2 \rightarrow$ formate	Cell-1: 0.1 M phosphate	Neutral PH
		Cell-2: formate → formaldehyde → methanol	Cell-2: —	25–400 mA cm^{-2}
	MPN@deCOP@Ag-Cu_2O; engineered *Escherichia coli* (ref. 49)	Cell-1: $CO_2 \rightarrow$ ethanol	Cell-1: 1.0 M KOH	Cell-1: 900 mA cm^{-2}
		Cell-2: ethanol → itaconic acid, isopropanol, and PHB	Cell-2: —	Cell-2: ADH, ALDH
	Cu–Ag; *Cupriavidus* necator (ref. 158)	Cell-1: $CO_2 \rightarrow C_2$ oxygenates	Cell-1: 0.1 M KH_2PO_4	Cell-1: 300 mA cm^{-2}
		Cell-2: C_2 oxygenates → PHB	Cell-2: —	Cell-2: pH 7.0
	C/Ag/carbon GDE (ref. 159)	Cell-1: $CO_2 \rightarrow CO$	Cell-1: 0.05 M H_2SO_4 + 3.0 M KCl	Cell-1: 100 mA
		Cell-2: CO → MCFAs	Cell-2: —	Cell-2: 35 °C, pH 6.2
	Cu/Cu_2O (ref. 160)	Cell-1: $CO_2 \rightarrow$ formate	Cell-1: 0.5 M $KHCO_3$	Cell-1: 50 mA
		Cell-2: formate → SCP	Cell-2: —	Cell-2: 37 °C

Nevertheless, confined cascade strategies still present notable limitations. Excessive confinement may suppress intermediate diffusion and poison active sites. Moreover, precisely constructing confined architectures with appropriate spatial dimensions, pore connectivity, and optimized interfacial chemistry remains challenging.[139] Combining confinement engineering with multiscale approaches enables the coordinated optimization of intermediate transport, interfacial mass transfer, and overall system stability. Table 3 summarizes the performance data for relevant confined cascade catalytic systems.

Tandem reactors

The strategy of tandem reactors enables the sequential integration of different reaction steps across multiple reactors, where the differential conditions between reactors (*e.g.*, pH, potential, and temperature) can be finely tuned to optimize the reaction environment. This approach enhances both the rate of target product formation and its selectivity.[46,146] For instance, Fig. 7a illustrates a cascaded electrolyzer system in which the reduction of CO_2 to CO and the subsequent reduction of CO to C_{2+} are coupled in different electrolyzers.[147] By creating tailored catalytic environments in each electrolyzer, this strategy significantly accelerates the production rate of C_{2+} products (Fig. 7b). Chi *et al.*[148] reported a dual electrolyzer cascade system: the first electrolyzer operates under alkaline conditions to electrochemically reduce CO_2 to ethanol, while the second electrolyzer, under acidic conditions, electrooxidizes ethanol and condenses it into the high-value six-carbon compound 1,1-diethoxyethane (DEE). This system achieves a highly efficient and selective conversion from CO_2 to multi-carbon products. The cascading reactor design not only greatly enhances product selectivity but also leads to efficient energy utilization and resource conversion.

Additionally, electrochemical reactors can be coupled with thermocatalytic and biocatalytic reactors, forming hybrid cascaded systems. This strategy effectively overcomes the limitations of single electrochemical transformations, improving reaction efficiency and enabling the synthesis of more complex, high-value products, thereby significantly enhancing the economic viability of the entire conversion process. For example, Chen *et al.*[149] proposed a cascaded electrochemical-thermochemical strategy in which C_2H_4 reacts with CO and H_2 to produce propanol and propionaldehyde (Fig. 7c and d). In this approach, CO_2 is first electrochemically reduced to C_2H_4, CO, and H_2, followed by a thermocatalytic hydrogenation–formylation reaction that converts these intermediates into C_3 oxygenated compounds. This cascading method achieves approximately 18% selectivity for C_3 products. Wang *et al.*[150] proposed a system that integrates electrochemical and biocatalytic processes on a gas diffusion electrode for the CO_2RR (Fig. 7e and f). Under neutral pH conditions, Ag-Bi_2O_3 selectively reduces gaseous CO_2 to carbonates, which are then further reduced to formaldehyde and methanol by formaldehyde dehydrogenase and alcohol dehydrogenase, respectively. This hybrid reactor cascade not only enhances reaction efficiency but also improves the overall selectivity and sustainability of the system. In summary, the tandem reactor strategy enhances the efficiency and selectivity of complex reactions at the macroscale by optimizing environmental conditions within each reactor and precisely controlling product distribution. Although tandem reactors can optimize reaction environments and regulate product distribution, diffusion limitations in intermediate transport between reactors, system operational complexity, and coupling interference between reaction conditions at different stages still constrain their precise control and efficiency enhancement for multistep reactions.[151] Therefore, integrating multiscale strategies to construct an integrated catalytic system featuring active sites, nanoconfinement, interfacial mass transfer, and reactor series connection enables efficient intermediate transport, thereby enhancing the overall efficiency of cascade reactions. Table 4 summarizes the catalytic performance of tandem reactors.

Conclusion and outlook

Based on the above, cascade electrocatalysis provides a novel pathway for the efficient conversion of carbon and nitrogen resources through atomic-scale catalyst design, nanoscale structural engineering, and macroscopic reactor integration. This review systematically summarizes the latest advancements

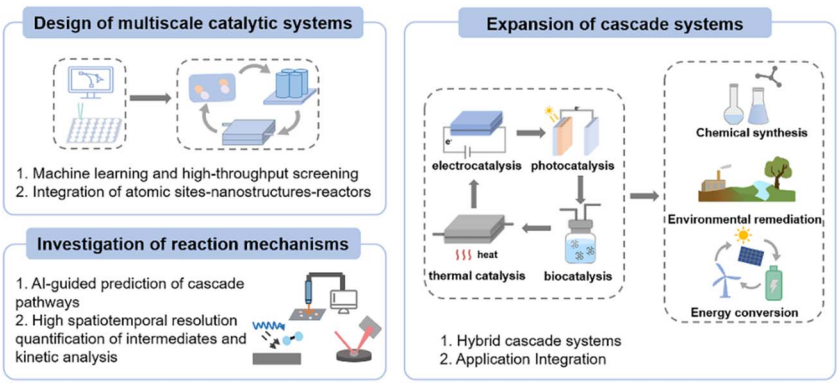

Fig. 8 Schematic illustration of future directions for the development of cascade electrocatalysis.

in this field, delving into the crucial role of the synergistic effects between single-atom/multi-atom sites at the atomic scale, interfacial and confinement effects at the sub-nanoscale and nanoscale, and reactor design at the macroscopic level in enhancing reaction activity and selectivity. Through multiscale cooperative effects, cascade electrocatalysis not only effectively reduces the energy barriers of reactions but also significantly improves reaction selectivity, especially in complex multistep reaction systems, demonstrating unique advantages. Despite substantial progress across various applications, cascade electrocatalysis continues to face several key challenges. Limited compatibility among different active sites constrains the sequential coupling required for efficient cascade pathways. The coexistence of multiple competing reaction routes further complicates selective control over the desired pathway. Moreover, the short lifetimes and low concentrations of critical intermediates hinder real-time detection and impede mechanistic elucidation. Nevertheless, with advances in cross-scale design strategies and *in situ* characterization techniques featuring high temporal and spatial resolution, cascade electrocatalysis is poised to offer broad opportunities for future applications (Fig. 8).

Design of multiscale catalytic systems

Cascade reactions involve multiple elementary steps and diverse intermediates, with overall efficiency constrained by the synergistic interplay of active site spatial distribution, mass transport processes, and electron transfer kinetics. Therefore, constructing catalysts with a multiscale framework is pivotal for enhancing the performance of cascade reactions. Future research will focus on the deep integration of artificial intelligence with experimental methods, employing machine learning models to predict and optimize the structural features of cascade catalysts. High-throughput synthesis and characterization platforms will be employed for rapid screening, thus establishing a closed-loop research and development cycle encompassing computational design, high-throughput fabrication and testing, and machine learning-driven optimization. The ultimate goal is to construct an integrated catalytic system spanning from atom-level active sites and nanoscale mass transport structures to reactor-scale engineering.

Investigation of reaction mechanisms

In cascade electrocatalysis, the dynamic evolution of complex intermediates and multiple reaction pathways presents significant challenges for real-time monitoring and mechanistic analysis. Future advancements may leverage artificial intelligence to predict possible reaction pathways and combine SI-SECM with *in situ* spectroscopic techniques such as infrared, Raman, and X-ray absorption spectroscopy to track the dynamic evolution of different active sites and the generation and consumption of intermediates in real time. This integrated approach will comprehensively reveal the intrinsic mechanisms and kinetic processes underlying cascade reactions.

Expansion of cascade systems

In single-mode electrocatalysis, driving complex multistep cascade reactions is often limited by low energy efficiency. Future developments will focus on hybrid catalytic systems that couple multiple energy fields, such as electrochemical-photonic, electrochemical-thermal, and electrochemical-biological coupling. By rationally designing and optimizing these multi-energy input, multi-reaction integrated systems, this approach should overcome the constraints of traditional single-mode catalysis, substantially expanding the scope of cascade catalysis for chemical synthesis, environmental remediation, and energy conversion. Such advances may enable higher selectivity, efficiency, and sustainability in complex molecule construction, deep pollutant transformation, and renewable energy utilization.

In summary, cascade electrocatalysis has been extensively explored for carbon–nitrogen resource utilization. With continued development in multiscale catalyst design, reaction mechanism investigation, and the integration of cascade systems, cascade electrocatalysis holds great promise for achieving more efficient resource conversion, thereby advancing the sustainable development of energy and the environment.

Author contributions

Writing – original draft, S. Li.; visualization, H. Li., R. Y., Y. P.; writing – review & editing, Z. J., P. Li.; funding acquisition, Z. J., P. Li.; supervision, P. Li, G. Y.

Conflicts of interest

There are no conflicts to declare.

Data availability

No primary research results, software or code have been included and no new data were generated or analysed as part of this review.

Acknowledgements

P. L. acknowledges funding support from the National Natural Science Foundation of China (22476141), the China Postdoctoral Science Foundation (2025M771235), and the Open Fund of Sichuan Engineering Technology Research Center for High Salt wastewater Treatment and Resource Utilization, Sichuan University of Science and Engineering (SCGCY-2403). G. Y. acknowledges the funding support from the Welch Foundation Award F-1861.

Notes and references

1 Y. Luo, K. Xie, P. Ou, C. Lavallais, T. Peng, Z. Chen, Z. Zhang, N. Wang, X.-Y. Li, I. Grigioni, B. Liu, D. Sinton, J. B. Dunn and E. H. Sargent, *Nat. Catal.*, 2023, **6**, 939–948.
2 E. T. A. Mitchard, *Nature*, 2018, **559**, 527–534.

3 P. H. van Langevelde, I. Katsounaros and M. T. M. Koper, *Joule*, 2021, **5**, 290–294.
4 C. Smith, A. K. Hill and L. Torrente-Murciano, *Energy Environ. Sci.*, 2020, **13**, 331–344.
5 W. Chen, X. Yang, Z. Chen, Z. Ou, J. Hu, Y. Xu, Y. Li, X. Ren, S. Ye, J. Qiu, J. Liu and Q. Zhang, *Adv. Funct. Mater.*, 2023, **33**, 2300512.
6 P. Li, Z. Jin, Z. Fang and G. Yu, *Energy Environ. Sci.*, 2021, **14**, 3522–3531.
7 S. Kuang, T. Xiao, H. Chi, J. Liu, C. Mu, H. Liu, S. Wang, Y. Yu, T. J. Meyer, S. Zhang and X. Ma, *Angew. Chem., Int. Ed.*, 2024, **63**, e202316772.
8 Y. Xiong, Y. Wang, J. Zhou, F. Liu, F. Hao and Z. Fan, *Adv. Mater.*, 2024, **36**, 2304021.
9 Y. Liu, K. Liu, P. Wang, Z. Jin and P. Li, *Carbon Neutrality*, 2023, **2**, 14.
10 M. Yi, H. Li, M. Xie, P. Li, Z. Jin and G. Yu, *Sci. China: Chem.*, 2025, **68**, 2322–2342.
11 T. Galimova, M. Ram, D. Bogdanov, M. Fasihi, A. Gulagi, S. Khalili and C. Breyer, *Renewable Sustainable Energy Rev.*, 2023, **183**, 113420.
12 W. Zhang, B. Jia, X. Liu and T. Ma, *SmartMat*, 2022, **3**, 5–34.
13 S. Guo, T. Asset and P. Atanassov, *ACS Catal.*, 2021, **11**, 5172–5188.
14 Y.-B. Huang, J. Liang, X.-S. Wang and R. Cao, *Chem. Soc. Rev.*, 2017, **46**, 126–157.
15 Y. Zhu, X. Cui, H. Liu, Z. Guo, Y. Dang, Z. Fan, Z. Zhang and W. Hu, *Nano Res.*, 2021, **14**, 4471–4486.
16 M. Duca, J. R. Weeks, J. G. Fedor, J. H. Weiner and K. A. Vincent, *ChemElectroChem*, 2015, **2**, 1086–1089.
17 R. D. Milton and S. D. Minteer, *ChemPlusChem*, 2017, **82**, 513–521.
18 C. Coelho and M. J. Romao, *Protein Sci.*, 2015, **24**, 1901–1911.
19 J. M. Carceller, K. S. Arias, M. J. Climent, S. Iborra and A. Corma, *Chem. Soc. Rev.*, 2024, **53**, 7875–7938.
20 C. Zhang, Q. Wang, Z. Li, H. Liu, L. Zhong, J. Liu, Z. Wang, R. Wu, P. Song, W. J. Chen, Z. Qi, C. Yan, L. Song, Q. Yan and C. Lv, *Angew. Chem., Int. Ed.*, 2025, **64**, e202502957.
21 X. Gao, C. Zhu and L. Zhang, *Chem Catal.*, 2025, **5**, 101544.
22 T. Yan, X. Chen, L. Kumari, J. Lin, M. Li, Q. Fan, H. Chi, T. J. Meyer, S. Zhang and X. Ma, *Chem. Rev.*, 2023, **123**, 10530–10583.
23 C. Liu, B. Qiao and T. Zhang, *JACS Au*, 2024, **4**, 4129–4140.
24 H. Yin, F. Dong, H. Su, Z. Zhuang, Y. Wang, D. Wang, Y. Peng and J. Li, *ACS Nano*, 2023, **17**, 25614–25624.
25 X. F. Cheng, J. H. He, H. Q. Ji, H. Y. Zhang, Q. Cao, W. J. Sun, C. L. Yan and J. M. Lu, *Adv. Mater.*, 2022, **34**, e2205767.
26 Y. Wang, P. Zhu, R. Wang, K. C. Matthews, M. Xie, M. Wang, C. Qiu, Y. Liu, H. Zhou, J. H. Warner, Y. Liu, H. Wang and G. Yu, *ACS Nano*, 2024, **18**, 26751–26758.
27 Z. Li, Y. Xie, Y. Han, H. Wang, J. Gao, L. Chen, L. Xu, L. Lu, Y. Zhao, E. Wang and G. Li, *Nano Res. Energy*, 2025, **4**, e9120169.
28 P. Li, R. Li, Y. Liu, M. Xie, Z. Jin and G. Yu, *J. Am. Chem. Soc.*, 2023, **145**, 6471–6479.
29 C. Wang, Z. Lv, X. Feng, W. Yang and B. Wang, *Adv. Energy Mater.*, 2024, **14**, 2400160.
30 J. Xiang, P. Wang, P. Li, M. Zhou, G. Yu and Z. Jin, *Angew. Chem., Int. Ed.*, 2025, **64**, e202500644.
31 S. Zhu, K. Liu, Z. Feng, H. Jiang and J. Lin, *Nano Res. Energy*, 2025, **4**, e9120188.
32 Y. Hu, J. Liu, W. Luo, J. Dong, C. Lee, N. Zhang, M. Chen, Y. Xu, D. Wu, M. Zhang, Q. Zhu, E. Hu, D. Geng, L. Zhong and Q. Yan, *Chem. Sci.*, 2024, **15**, 8204–8215.
33 G. Xie, W. Guo, Z. Fang, Z. Duan, X. Lang, D. Liu, G. Mei, Y. Zhai, X. Sun and X. Lu, *Angew. Chem., Int. Ed.*, 2024, **63**, e202412568.
34 J. Yan, J. Li, P. Liu, H. Huang and W. Song, *Green Chem.*, 2023, **25**, 8645–8651.
35 Y. Wang, H. Su, Y. He, L. Li, S. Zhu, H. Shen, P. Xie, X. Fu, G. Zhou, C. Feng, D. Zhao, F. Xiao, X. Zhu, Y. Zeng, M. Shao, S. Chen, G. Wu, J. Zeng and C. Wang, *Chem. Rev.*, 2020, **120**, 12217–12314.
36 K. Liu, J. Li, Y. Liu, M. Wang and H. Cui, *J. Energy Chem.*, 2023, **79**, 515–534.
37 K. Liu, Z. Sun, X. Peng, X. Liu, X. Zhang, B. Zhou, K. Yu, Z. Chen, Q. Zhou, F. Zhang, Y. Wang, X. Gao, W. Chen and P. Chen, *Nat. Commun.*, 2025, **16**, 2167.
38 Y. Cheng, Q. Li, M. I. B. Salaman, C. Wei, Q. Wang, X. Ma, B. Liu and A. B. Wong, *J. Am. Chem. Soc.*, 2025, **147**, 12438–12448.
39 M. Melchionna, P. Fornasiero, M. Prato and M. Bonchio, *Energy Environ. Sci.*, 2021, **14**, 5816–5833.
40 Y. Zhang, F. Chen, X. Hao, Y. Liu, W. Wu, X. Zhang, Z. Zang, H. Dong, W. Wang, F. Lu, Z. Lu, H. Liu, H. Liu, F. Luo and Y. Cheng, *Appl. Catal., B*, 2024, **344**, 123666.
41 Y. Xu, K. Shi, T. Ren, H. Yu, K. Deng, X. Wang, Z. Wang, H. Wang and L. Wang, *Small*, 2022, **18**, 2203335.
42 H. Liu, L. An, P. Wang, C. Yu, J. Zhang, H. Shin, B. Peng, J. Li, M. Li, H. An, J. Yu, Y. Chen, P. Wang, K.-S. Lee, K. Lalit, Z. Liu, O. K. Farha, W. Huang, J. Z. Liu, L. Qi, K. Xie and E. H. Sargent, *Nat. Commun.*, 2025, **16**, 6185.
43 C. Bie, J. Yang, X. Zeng, Z. Wang, X. Sun, Z. Yang, J. Yu and X. Zhang, *Small*, 2025, **21**, e2411184.
44 G. Shi, W. Zhang, Y. Kang, J. Zhao, T. Lu, C. Yang, M. Chang, Y. Shen, X. Gao, J. Wu, Y.-F. Li, K. Cao and L. Zhang, *Nat. Commun.*, 2025, **16**, 7359.
45 W. Qiu, P. Wang, Z. Jin, W. Liu, P. Li and Z. Pan, *Appl. Catal., B*, 2025, **367**, 125102.
46 M. Wang, W. Fang, D. Zhu, C. Xia, W. Guo and B. Y. Xia, *Chin. J. Catal.*, 2025, **69**, 1–16.
47 A. Ozden, Y. Wang, F. Li, M. Luo, J. Sisler, A. Thevenon, A. Rosas-Hernández, T. Burdyny, Y. Lum, H. Yadegari, T. Agapie, J. C. Peters, E. H. Sargent and D. Sinton, *Joule*, 2021, **5**, 706–719.
48 G. Mei, Y. Lu, X. Yang, S. Chen, X. Yang, L. M. Yang, C. Tang, Y. Sun, B. Y. Xia and B. You, *Angew. Chem., Int. Ed.*, 2024, **63**, e202314708.
49 L. Han, Y. Li, X. Wang, Z. Yao, Z. Chen, J. p. Li, T. Tan, S. Y. Lee and Y. Lv, *Adv. Energy Mater.*, 2025, **15**, e03056.
50 Y. Liu, X. Su, J. Ding, J. Zhou, Z. Liu, X. Wei, H. B. Yang and B. Liu, *Chem. Soc. Rev.*, 2024, **53**, 11850–11887.

51 S. K. Beaumont, *Phys. Chem. Chem. Phys.*, 2020, **22**, 18747–18756.
52 Z. Jin, R. Guan, X. Li, D. Yuan and P. Li, *Chin. Chem. Lett.*, 2025, **36**, 110506.
53 Q. Xu, J. A. Zamora Zeledon, B. O. Joensen, L. Trotochaud, A. Sartori, L. M. Kaas, A. B. Moss, M. Mirolo, L. Mairena, S. Huynh, S. Garg, S. Helveg, I. Chorkendorff, S. Zhao, B. Seger and J. Drnec, *Nat. Nanotechnol.*, 2025, **20**, 889–896.
54 Y.-Y. Lou, Q.-Z. Zheng, S.-Y. Zhou, J.-Y. Fang, O. Akdim, X.-Y. Ding, R. Oh, G.-S. Park, X. Huang and S.-G. Sun, *ACS Catal.*, 2024, **14**, 5098–5108.
55 Y. Dai, S. Li, X. Li, K. Liu, Y. Guo, H. Li and B. Jiang, *Adv. Funct. Mater.*, 2025, **35**, 2420282.
56 X.-X. Fu, H. Guo, D.-H. Si, H.-J. Zhu, Y.-Y. Lan, Y.-B. Huang and R. Cao, *Chem. Sci.*, 2025, **16**, 13503–13513.
57 J. Ding, L. Liu, J. Zhang, Y. Liu, H. Xu, Z. Shen, H. B. Yang, X. Feng, Y. Huang and B. Liu, *J. Am. Chem. Soc.*, 2025, **147**, 9601–9609.
58 W. Shen, Y. Ye, Q. Xia and P. Xi, *EES Catal.*, 2025, **3**, 10–31.
59 K. Chen, F. Wang, X. Lu, Y. Li and K. Chu, *ACS Catal.*, 2023, **13**, 9550–9557.
60 A. Prajapati, C. Hahn, I. M. Weidinger, Y. Shi, Y. Lee, A. N. Alexandrova, D. Thompson, S. R. Bare, S. Chen, S. Yan and N. Kornienko, *Nat. Commun.*, 2025, **16**, 2593.
61 J. Song, Z.-X. Qian, J. Yang, X.-M. Lin, Q. Xu and J.-F. Li, *ACS Energy Lett.*, 2024, **9**, 4414–4440.
62 Z. Yao, C. Lin, J. Gao, J. Feng, M. Li, W. Yan, W. Zhang and H. Wang, *Appl. Catal., B*, 2025, **378**, 125550.
63 J. Xu, R. Chen, J. Song, S. Liu, Y. Shen and Y. Zhang, *Chem. Sci.*, 2025, **16**, 9564–9576.
64 H. Li, Y. Guo and Z. Jin, *Carbon Neutrality*, 2023, **2**, 22.
65 L. He, Z. Cai, C. Wang, L. Yang, W. Yong and Z. Jin, *Adv. Funct. Mater.*, 2025, e14592.
66 Z. Jin, *Anal. Chem.*, 2023, **95**, 6477–6489.
67 P. Wang, P. Li, Z. Pan, K. Liu, M. Xie, L. Zhou, M. Zhou, G. Yu and Z. Jin, *Nat. Commun.*, 2025, **16**, 5581.
68 R. Yang, L. Yang, W. Yong, P. Li, M. Zhou and Z. Jin, *Chem. Sci.*, 2025, **16**, 18482–18495.
69 W. He, J. Zhang, S. Dieckhöfer, S. Varhade, A. C. Brix, A. Lielpetere, S. Seisel, J. R. C. Junqueira and W. Schuhmann, *Nat. Commun.*, 2022, **13**, 1129.
70 L. Xiao, G. Wang, X. Huang, S. Zhou, R. Zhou, Y. Jiang, S. Liu, G. Li, H. Zheng, S.-G. Sun and H.-G. Liao, *Appl. Catal., B*, 2022, **307**, 121164.
71 Q. Zhang, Z. Song, X. Sun, Y. Liu, J. Wan, S. B. Betzler, Q. Zheng, J. Shangguan, K. C. Bustillo, P. Ercius, P. Narang, Y. Huang and H. Zheng, *Nature*, 2024, **630**, 643–647.
72 T.-H. Shen, R. Girod, J. Vavra and V. Tileli, *J. Electrochem. Soc.*, 2023, **170**, 056502.
73 Y. Yao, Z. Sun, T. Li, Z. Zhao, Z. Li, X. Lu, Y. Wan, Y. Fan and Z. Chen, *ACS Nano*, 2025, **19**, 18947–18975.
74 X. Peng, L. Zeng, D. Wang, Z. Liu, Y. Li, Z. Li, B. Yang, L. Lei, L. Dai and Y. Hou, *Chem. Soc. Rev.*, 2023, **52**, 2193–2237.
75 Y. Zhou, G. Xing, C. Sun, Z. Chen, S. Li, R. Yang, M. Chen, P. Zhang, C. Feng, A. Abudula and G. Guan, *Adv. Funct. Mater.*, 2025, e15635.
76 W. Qiu, Y. Liu, M. Xie, Z. Jin, P. Li and G. Yu, *EES Catal.*, 2024, **2**, 202–219.
77 X. Liang, H. Zhu, X. Yang, S. Xue, Z. Liang, X. Ren, A. Liu and G. Wu, *Small Struct.*, 2022, **4**, 2200202.
78 T. Yang, M. Kuang and J. Yang, *Nano Res.*, 2023, **16**, 8670–8683.
79 J. Li, Z. Wang, C. McCallum, Y. Xu, F. Li, Y. Wang, C. M. Gabardo, C.-T. Dinh, T.-T. Zhuang, L. Wang, J. Y. Howe, Y. Ren, E. H. Sargent and D. Sinton, *Nat. Catal.*, 2019, **2**, 1124–1131.
80 X. Kong, J. Zhao, J. Ke, C. Wang, S. Li, R. Si, B. Liu, J. Zeng and Z. Geng, *Nano Lett.*, 2022, **22**, 3801–3808.
81 L. Lv, H. Tan, Y. Kong, B. Tang, Q. Ji, Y. Liu, C. Wang, Z. Zhuang, H. Wang, M. Ge, M. Fan, D. Wang and W. Yan, *Angew. Chem., Int. Ed.*, 2024, **63**, e202401943.
82 Y. Wan, M. Zheng, W. Yan, J. Zhang and R. Lv, *Adv. Energy Mater.*, 2024, **14**, 2303588.
83 Y. Zhang, Z. Li, K. Chen, X. Yang, H. Zhang, X. Liu and K. Chu, *Adv. Energy Mater.*, 2024, **14**, 2402309.
84 J. M. Moore and A. R. Fout, *Chem. Sci.*, 2025, **16**, 840–845.
85 S. Tian, R. Wu, H. Liu, C. Yan, Z. Qi, P. Song, W. J. Chen, L. Song, Z. Wang and C. Lv, *Angew. Chem., Int. Ed.*, 2025, **64**, e202510665.
86 J. Liu, Y. Xu, R. Duan, M. Zhang, Y. Hu, M. Chen, B. Han, J. Dong, C. Lee, L. S. R. Kumara, O. Seo, J. Tseng, T. Watanabe, Z. Liu, Q. Zhu, J. Xu, M.-F. Ng, D. Wu and Q. Yan, *Nat. Commun.*, 2025, **16**, 3595.
87 Z. Wu, Y. Song, H. Guo, F. Xie, Y. Cong, M. Kuang and J. Yang, *Interdiscip. Mater.*, 2024, **3**, 245–269.
88 B. Kang, B. Xu, Z. Chen, F. Li and Y. Wang, *Appl. Catal., B*, 2025, **360**, 124528.
89 X. You, J. Xu, Z. Zhuang, J. Xia, S. Wang, H. Wei, Y. Li, Y. Cai, H. Xiang and B. Yu, *Nano Res.*, 2024, **17**, 4815–4824.
90 M. Xie, S. Tang, Z. Li, M. Wang, Z. Jin, P. Li, X. Zhan, H. Zhou and G. Yu, *J. Am. Chem. Soc.*, 2023, **145**, 13957–13967.
91 Z. Liu, C. Xing, Y. Shan, M. Ma, S. Wu, R. Ge, Q. Xue and J. Tian, *Chem. Sci.*, 2025, **16**, 7010–7017.
92 C.-H. Shen, Y. Zhao, H. N. Nam, L. Zhu, Q. M. Phung, V. Austen, M. Kim, D. Jiang, X. Wei, T. Yokoshima, C.-W. Kung and Y. Yamauchi, *Chem. Sci.*, 2025, **16**, 7026–7038.
93 L. Qin, F. Sun, Z. Gong, G. Ma, Y. Chen, Q. Tang, L. Qiao, R. Wang, Z.-Q. Liu and Z. Tang, *ACS Nano*, 2023, **17**, 12747–12758.
94 K. Liu, H. Li, M. Xie, P. Wang, Z. Jin, Y. Liu, M. Zhou, P. Li and G. Yu, *J. Am. Chem. Soc.*, 2024, **146**, 7779–7790.
95 Z. Jin, K. Liu, Z. Pan, X. Shan, F. Cai, D. Yang, P. Li, G. Yu and M. Zhou, *J. Am. Chem. Soc.*, 2025, DOI: 10.1021/jacs.5c15278.
96 C. Du, J. P. Mills, A. G. Yohannes, W. Wei, L. Wang, S. Lu, J.-X. Lian, M. Wang, T. Guo, X. Wang, H. Zhou, C.-J. Sun, J. Z. Wen, B. Kendall, M. Couillard, H. Guo, Z. Tan, S. Siahrostami and Y. A. Wu, *Nat. Commun.*, 2023, **14**, 6142.
97 J. Li, Y. Chen, B. Yao, W. Yang, X. Cui, H. Liu, S. Dai, S. Xi, Z. Sun, W. Chen, Y. Qin, J. Wang, Q. He, C. Ling, D. Wang and Z. Zhang, *J. Am. Chem. Soc.*, 2024, **146**, 5693–5701.

98 J. Zhong, H. Duan, M. Cai, Y. Zhu, Z. Wang, X. Li, Z. Zhang, W. Qu, K. Zhang, D. Han, D. Cheng, Y. Shen, M. Xie, E. Cortes and D. Zhang, *Angew. Chem., Int. Ed.*, 2025, **64**, e202507956.
99 W. Ye, Y. Yao, X. Wei, M. Xu, S. Zhao, W. Wang, G. Jia, F. Dai, P. Gao, X. Lu, X. Li, B. Xi, N. Wang and S. Xiong, *Angew. Chem., Int. Ed.*, 2025, **64**, e202509303.
100 B. Kim, Y. C. Tan, Y. Ryu, K. Jang, H. G. Abbas, T. Kang, H. Choi, K.-S. Lee, S. Park, W. Kim, P.-P. Choi, S. Ringe and J. Oh, *ACS Energy Lett.*, 2023, **8**, 3356–3364.
101 Y. Zhang, P. Li, C. Zhao, G. Zhou, F. Zhou, Q. Zhang, C. Su and Y. Wu, *Sci. Bull.*, 2022, **67**, 1679–1687.
102 S. A. Chala, R. Liu, E. O. Oseghe, S. T. Clausing, C. Kampf, J. Bansmann, A. H. Clark, Y. Zhou, I. Lieberwirth, J. Biskupek, U. Kaiser and C. Streb, *ACS Catal.*, 2024, **14**, 15553–15564.
103 C. Jin, Y. Lin, Y. Wang, J. Shi, R. Li, Y. Liu, Z. Yue, K. Leng, Y. Zhao, Y. Wang, X. Han, Y. Qu and J. Bai, *Adv. Mater.*, 2025, **37**, 2412658.
104 W. Du, Z. Sun, S. Shang, K. Chen, X. Yang and K. Chu, *ACS Nano*, 2024, **18**, 27718–27726.
105 Y. Gao, J. Wang, M. Sun, Y. Jing, L. Chen, Z. Liang, Y. Yang, C. Zhang, J. Yao and X. Wang, *Angew. Chem., Int. Ed.*, 2024, **63**, e202402215.
106 K. Chen, D. Ma, Y. Zhang, F. Wang, X. Yang, X. Wang, H. Zhang, X. Liu, R. Bao and K. Chu, *Adv. Mater.*, 2024, **36**, e2402160.
107 X. Wu, Y. Chen, B. Tang, Q. Yan, D. Wu, H. Zhou, H. Wang, H. Zhang, D. He, H. Li, J. Zeng, L. Lu, S. Yang and T. Ma, *Nat. Commun.*, 2025, **16**, 8785.
108 J. Lim, C.-Y. Liu, J. Park, Y.-H. Liu, T. P. Senftle, S. W. Lee and M. C. Hatzell, *ACS Catal.*, 2021, **11**, 7568–7577.
109 Z. Li, M. Zheng, C. Yan, D. Yang, R. Yang, C. Zhang, H. Liu, P. Song, C. Yin, Z. Qi, D. Liu, X. Zhou, L. Song, C. Lv and G. Yu, *Nat. Commun.*, 2025, **16**, 8940.
110 S. Bhowmick, A. Adalder, A. Maiti, S. Kapse, R. Thapa, S. Mondal and U. K. Ghorai, *Chem. Sci.*, 2025, **16**, 4806–4814.
111 Y. Fu, S. Wang, Y. Wang, P. Wei, J. Shao, T. Liu, G. Wang and X. Bao, *Angew. Chem., Int. Ed.*, 2023, **62**, e202303327.
112 S. Chen, Z. Zhu, K. Song, H. Zhang, D. Luo, T. Cao, Y. Zou, C. Liu, L. Gan, D. Zhang, Y. Han and J. Huang, *J. Am. Chem. Soc.*, 2025, **147**, 36494–36507.
113 W. Ye, Y. Zhang, L. Chen, F. Wu, Y. Yao, W. Wang, G. Zhu, G. Jia, Z. Bai, S. Dou, P. Gao, N. Wang and G. Wang, *Angew. Chem., Int. Ed.*, 2024, **63**, e202410105.
114 Z. Li, Z. Shi, Y. Ou, L. Zhong, C. Yan, C. Zhang, K. Song, H. Liu, D. Liu, P. Song, C. Yin, Z. Qi, L. Song and C. Lv, *Angew. Chem., Int. Ed.*, 2025, **64**, e202510287.
115 C. Zhang, Q. Zhou, Z. Li, C. Yan, H. Liu, D. Liu, L. Song, Q. Yan and C. Lv, *Angew. Chem., Int. Ed.*, 2025, **64**, e202507869.
116 X. Gao, C. Zhu, C. Yang, G. Shi, Q. Xu and L. Zhang, *ACS Catal.*, 2024, **14**, 17871–17878.
117 Y. Ma, L. Guo, L. Chang, W. Guo, T. Zhou, F. Hao, W. Su, J. Zhou, G. Wang, M. Shao, J. Yu, J. Yin, Y. Wang, F. Liu, A. Zhang, K. Qian, J. Wang, X. Zhang, W. Zhou, S. Chu, C. Ling, L. Gan, Z. Guo and Z. Fan, *Nat. Commun.*, 2025, **16**, 7632.
118 Z. Li, Q. Wang, L. Zhong, C. Yan, Z. Shi, Y. Ou, Y. Shang, C. Zhang, S. Tian, H. Liu, D. Liu, P. Song, Z. Qi, L. Song and C. Lv, *Mater. Today*, 2025, **85**, 49–59.
119 Y. Chen, X. Liu, S. Li, J. Li, M. Fan and S. Shu, *Adv. Funct. Mater.*, 2025, e21409.
120 Y. Dang, R. Zhang, S. Ren, S. Pitchaimuthu, S. Liu, R. Xing and X. Yang, *Chem. Eng. J.*, 2025, **520**, 166370.
121 Y. Tang, S. Liu, C. Guo, Y. Liu and Z. Tang, *Sustainable Energy Fuels*, 2023, **7**, 5039–5045.
122 Y. Shi, Y. Wang, J. Yu, Y. Chen, C. Fang, D. Jiang, Q. Zhang, L. Gu, X. Yu, X. Li, H. Liu and W. Zhou, *Adv. Energy Mater.*, 2023, **13**, 2203506.
123 Z. Zhang, X. Ma, Y. Song, X. Yang, Q. Fang, Y. Yamauchi and J. Tang, *Angew. Chem., Int. Ed.*, 2025, **64**, e202511704.
124 C. Zhu, L. Zhou, Z. Zhang, C. Yang, G. Shi, S. Zhao, H. Gu, J. Wu, X. Gao, Y. Li, K. Liu, S. Dai and L. Zhang, *Chem*, 2022, **8**, 3288–3301.
125 C. Zhu, Z. Zhang, R. Qiao, C. Yang, S. Zhao, G. Shi, X. Gao, H. Gu, K. Liu and L. Zhang, *J. Phys. Chem. C*, 2023, **127**, 3470–3477.
126 Z.-x. Yang, X. Wen, L.-j. Gao, J. Zhang, R.-p. Wei, X.-m. Pan and G.-m. Xiao, *Catal. Commun.*, 2023, **174**, 106595.
127 Y. Ma, J. Yu, M. Sun, B. Chen, X. Zhou, C. Ye, Z. Guan, W. Guo, G. Wang, S. Lu, D. Xia, Y. Wang, Z. He, L. Zheng, Q. Yun, L. Wang, J. Zhou, P. Lu, J. Yin, Y. Zhao, Z. Luo, L. Zhai, L. Liao, Z. Zhu, R. Ye, Y. Chen, Y. Lu, S. Xi, B. Huang, C. S. Lee and Z. Fan, *Adv. Mater.*, 2022, **34**, e2110607.
128 X. Gao, Y. Jiang, J. Liu, G. Shi, C. Yang, Q. Xu, Y. Yun, Y. Shen, M. Chang, C. Zhu, T. Lu, Y. Wang, G. Du, S. Li, S. Dai and L. Zhang, *Nat. Commun.*, 2024, **15**, 10331.
129 J. Tan, Q. Shen, X. Jin, M. Wang, B. A, W. Chen, Z. Wei, L. Zhang and J. Shi, *J. Am. Chem. Soc.*, 2025, **147**, 23635–23642.
130 Z. Cai, N. Cao, F. Zhang, X. Lv, K. Wang, Y. He, Y. Shi, H. Bin Wu and P. Xie, *Appl. Catal., B*, 2023, **325**, 122310.
131 Y. Chen, X. Y. Li, Z. Chen, A. Ozden, J. E. Huang, P. Ou, J. Dong, J. Zhang, C. Tian, B. H. Lee, X. Wang, S. Liu, Q. Qu, S. Wang, Y. Xu, R. K. Miao, Y. Zhao, Y. Liu, C. Qiu, J. Abed, H. Liu, H. Shin, D. Wang, Y. Li, D. Sinton and E. H. Sargent, *Nat. Nanotechnol.*, 2024, **19**, 311–318.
132 Y. Yu, D. Wang, Y. Hong, T. Zhang, C. Liu, J. Chen, G. Qin and S. Li, *Chem. Commun.*, 2022, **58**, 11163–11166.
133 C. Lv, C. Lee, L. Zhong, H. Liu, J. Liu, L. Yang, C. Yan, W. Yu, H. H. Hng, Z. Qi, L. Song, S. Li, K. P. Loh, Q. Yan and G. Yu, *ACS Nano*, 2022, **16**, 8213–8222.
134 R. Qi, Q. Jiang, L. Deng, X. Yu, B. Shi, M. Zhong, Y. Wang and X. Lu, *Chem. Sci.*, 2025, **16**, 378–385.
135 M. Li, C. Qi, J. Xu, R. Zou, L. Wang, W. Jiang, Y. Fan, P. Qiu and W. Luo, *ACS Nano*, 2025, **19**, 11309–11322.
136 Y. Lu, H. Li, H. Sun, J. Zhao, Y. Zhang, Y. Wang, C. Zhu, D. Gao, Y. Tuo, J. Zeng, D. Chen and Z. Yan, *ACS Catal.*, 2024, **14**, 14744–14753.

137 D. Zhang, D. Jiang, B. Mao, Y. Liu, Q. Chen, H. Li, L. Xing, H. Huang, W. Zhang, W. Shi and Z. Kang, *Angew. Chem., Int. Ed.*, 2025, **64**, e202511259.
138 W. Huang, W. Luo, J. Liu, B.-E. Jia, C. Lee, J. Dong, L. Yang, B. Liu and Q. Yan, *ACS Nano*, 2024, **18**, 20258–20267.
139 L. Chen, M. Li and J.-N. Zhang, *Nano Res.*, 2024, **17**, 7880–7899.
140 B. Zhang, Y. Hou, S. Wang, S. Zhou, Z. Li, Y. Hou, L. Lei and B. Yang, *Appl. Catal., B*, 2025, **379**, 125727.
141 J. Li, Q. Zhu, A. Chang, S. Cheon, Y. Gao, B. Shang, H. Li, C. L. Rooney, L. Ren, Z. Jiang, Y. Liang, Z. Feng, S. Yang, L. Robert Baker and H. Wang, *Nat. Nanotechnol.*, 2025, **20**, 515–522.
142 J. Chen, D. Wang, X. Yang, W. Cui, X. Sang, Z. Zhao, L. Wang, Z. Li, B. Yang, L. Lei, J. Zheng, L. Dai and Y. Hou, *Angew. Chem., Int. Ed.*, 2023, **62**, e202215406.
143 F. Yu, X. Liu, L. Liao, G. Xia and H. Wang, *Small*, 2023, **19**, e2301558.
144 H. Pan, J. Wu, X. Lu, Y. Li, Q. Zhang, J. Ling, Y. Wang and B. Min, *ACS Appl. Energy Mater.*, 2025, **8**, 8299–8310.
145 X. Yu, S. Zeng, R. Li, X. Dong, Q. Cao, L. Li and X. Guo, *Chem. Eng. J.*, 2025, **519**, 165559.
146 M. Liu, X. Lu, R. He, Y. Zhou, Y. Liu, L. Chen, X. Suo, J. Hou, Q. Ke, Z. Chen, P. Feng and C. Wan, *Chem. Eng. J.*, 2025, **523**, 168293.
147 T. Möller, M. Filippi, S. Brückner, W. Ju and P. Strasser, *Nat. Commun.*, 2023, **14**, 5680.
148 H. Chi, Z. Liang, S. Kuang, Y. Jin, T. Xiao, J. Lin, D. Han, L. Wang, S. Zhang and X. Ma, *J. Am. Chem. Soc.*, 2025, **147**, 32640–32648.
149 A. N. Biswas, Z. Xie, R. Xia, S. Overa, F. Jiao and J. G. Chen, *ACS Energy Lett.*, 2022, **7**, 2904–2910.
150 P. Wang, X. Wang, S. Chandra, A. Lielpetere, T. Quast, F. Conzuelo and W. Schuhmann, *Angew. Chem., Int. Ed.*, 2025, **64**, e202422882.
151 J. Feng, A. Badreldin and Y. Li, *Energy Fuels*, 2025, **39**, 21175–21225.
152 G. Wu, Y. Song, Q. Zheng, C. Long, T. Fan, Z. Yang, X. Huang, Q. Li, Y. Sun, L. Zuo, S. Lei and Z. Tang, *Adv. Energy Mater.*, 2022, **12**, 2202054.
153 H. Li, H. Li, P. Wei, Y. Wang, Y. Zang, D. Gao, G. Wang and X. Bao, *Energy Environ. Sci.*, 2023, **16**, 1502–1510.
154 J. Weidner, C. N. Tchassem, D. Das, R. Zerdoumi, G. Lu, X. Wang, M. Muhler, N. Sikdar and W. Schuhmann, *ChemElectroChem*, 2025, **12**, e202400664.
155 Z. Xie, E. Huang, S. Garg, S. Hwang, P. Liu and J. G. Chen, *Nat. Catal.*, 2024, **7**, 98–109.
156 H. Lv, X. Dong, R. Li, C. Zeng, X. Zhang, Y. Song, H. Liu, J. Shao, N. Ta, Q. Zhao, Q. Fu, J. Xiao, G. Wang and X. Bao, *Nat. Chem.*, 2025, **17**, 695–702.
157 S. Garg, Z. Xie, A. X. Lam and J. G. Chen, *ACS Energy Lett.*, 2024, **9**, 2990–2996.
158 G. Lee, H. J. Jo, J. Choi, M. F. Guzman, Y. Shan, H. K. D. Le, J. Feijoo, N. Soland, D. S. Clark and P. Yang, *Proc. Natl. Acad. Sci. U. S. A.*, 2025, **122**, e2512565122.
159 Y. Pu, Y. Wang, G. Wu, X. Wu, Y. Lu, Y. Yu, N. Chu, X. He, D. Li, R. J. Zeng and Y. Jiang, *Environ. Sci. Technol.*, 2024, **58**, 7445–7456.
160 H. Cui, W. Liu, C. Ma, P. Shiri, Z. Zhu, H. Jiang, D. Li and L. Zhang, *Appl. Catal., B*, 2024, **350**, 123946.